Long-term variability of the optical spectra of NGC 4151: I. Light curves and flux correlations.

A.I. Shapovalova[1], L.Č. Popović[2,3], S. Collin[4], A.N. Burenkov[1], V.H. Chavushyan[5], N.G. Bochkarev[6], E. Benítez[7], D. Dultzin-Hacyan[7], A. Kovačević[8], N. Borisov[1], L. Carrasco[5], J. León-Tavares[5,9], A. Mercado[10], J.R. Valdes[5], V.V. Vlasuyk[1], and V.E. Zhdanova[1]

[1] Special Astrophysical Observatory of the Russian AS, Nizhnij Arkhyz, Karachaevo-Cherkesia 369167, Russia
[2] Astronomical Observatory, Volgina 7, 11160 Belgrade 74, Serbia
[3] Alexander von Humboldt Fellow, presently at Max Planck Institute for Radioastronomy, Bonn, Germany
[4] LUTH, Observatoire de Paris, CNRS, Université Paris Diderot; 5 Place Jules Janssen, 92190 Meudon, France
[5] Instituto Nacional de Astrofísica, Óptica y Electrónica, Apartado Postal 51, CP 72000, Puebla, Pue. México
[6] Sternberg Astronomical Institute, Moscow, Russia
[7] Instituto de Astronomía, UNAM, Apartado Postal 70-264, CP 04510, México
[8] Department of Astronomy, Faculty of Mathematics, University of Belgrade, Studentski trg 16, 11000 Belgrade, Serbia
[9] Max-Planck Institute für Radioastronomie, Auf dem Hügel 69, 53121 Bonn, Germany
[10] Universidad Politécnica de Baja California, Av. de la Industria # 291, CP 21010, Mexicali, B.C., México

Received / Accepted

ABSTRACT

Aims. Results of a long-term spectral monitoring of the active galactic nucleus of NGC 4151 are presented (11 years, from 1996 to 2006).
Methods. High quality spectra (S/N> 50 in the continuum near Hα and Hβ) were obtained in the spectral range ~ 4000 to 7500 Å, with a resolution between 5 and 15 Å, using the 6-m and the 1-m SAO's telescopes (Russia), the GHAO's 2.1-m telescope (Cananea, México), and the OAN-SPM's 2.1-m telescope (San-Pedro, México). The observed fluxes of the Hα, Hβ, Hγ and HeIIλ4686 emission lines and of the continuum at the observed wavelength 5117Å, were corrected for the position angle, the seeing and the aperture effects.
Results. We found that the continuum and line fluxes varied strongly (up to a factor 6) during the monitoring period. The emission was maximum in 1996-1998, and there were two minima, in 2001 and in 2005. As a consequence, the spectral type of the nucleus changed from a Sy1.5 in the maximum activity state to a Sy1.8 in the minimum state. The Hα, Hγ and Heλ4686 fluxes were well correlated with the Hβ flux. The line profiles were strongly variable, showing changes of the blue and red asymmetry. The flux ratios of the blue/red wings and of the blue (or red) wing/core of Hα and Hβ varied differently. We considered three characteristic periods during which the Hβ and Hα profiles were similar: 1996-1999, 2000-2001 and 2002-2006. The line to continuum flux ratios were different; in particular during the first period (1996-2001), the lines were not correlated with the continuum and saturated at high fluxes. In the third period (2002-2006), the Hα and Hβ fluxes were well correlated to the continuum flux, meaning that the ionizing continuum was a good extrapolation of the optical continuum. We thus consider that the values of the time lags – **line lagging continuum** ($0.81^{+1.55}_{-0.81}$ **days** for Hα and $0.81^{+2.19}_{-0.81}$ **days** for Hβ) for the third period give a more realistic estimation of the dimension of the BLR than during the other periods. **Moreover, the time lags obtained by binning intervals of three years within the whole monitoring period indicate the permanent presence of a small component of the BLR (0.3-0.7 light days)**
Conclusions. We discuss the different responses of Hβ and Hα to the continuum during the monitoring period.

Key words. galaxies: active - galaxies: individual: NGC 4151

1. Introduction

The brightest Seyfert 1.5-type galaxy NGC 4151 has been studied in detail at all wavelengths (e.g. Peterson 1988 and Ulrich 2000) The nucleus of this galaxy shows flux variability in a wide wavelength range, with time-scales from a few hours (in the hard X-ray, e.g. Yaqoob et al. 1993) to several months (in the infrared, e.g. Oknyanskij et al. 1999).

In the optical range, the Active Galactic Nucleus (AGN) of this galaxy is also known to display flux variations of the continuum and of the lines up to a factor ten or more (e.g. Peterson

1988, Clavel et al. 1990, Maoz et al. 1991, Shapovalova et al. 1996, Ulrich & Horne 1996, Sergeev et al. 2001, Lyuty 2005). These variations occur in time scales of several days (Maoz et al. 1991).

NGC 4151 has been the subject of echo-mapping observational campaigns. The main aim of AGN monitoring campaigns was to determine the size of the Broad Line Region (BLR) by measuring the time delay between the emission line fluxes, in response to the variations of the continuum flux (see Peterson 1993 for a review). It is interesting that different authors found different time lags: Antonucci & Cohen (1983) observed NGC 4151 at least once a month from 1980 May through 1981 July, and found that the BLR radius was less than 30 lt-days. These observations were also used by Peterson & Cota (1988) in com-

bination with their own observations (performed from 1985 to 1986), and they found a BLR radius of 6 ± 4 lt-days. Gaskell & Sparke (1986) applied the cross-correlation method to the ultraviolet data of Ulrich et al. (1984) and to the optical data of Antonucci & Cohen (1983), and they found a BLR size between 2 lt-days (for HeIIλ4686) and 20 lt-days (for Hα).

On the other hand, Maoz et al. (1991) analyzed the observations (optical continuum, Hβ and Hα) from 67 nights during a 216-day period between December 15, 1987, and July 18, 1988, and they found a BLR size of 9 ± 2 lt-days. They also showed that in a time-scale of 0 ± 5 days, the wings of Hα and Hβ varied in phase, and they ruled out a pure unidirectional radial motion in the BLR (either inflow or outflow).

A 10–years long monitoring campaign (1988-1998) of the NGC 4151 nucleus was performed with a sampling of 1-2 observations per month, using the CCD spectrograph of the 2.6-m CrAO telescope which covers the Hα and Hβ spectral range (Malkov et al. 1997, Sergeev et al. 2001). The time delays between the broad lines and the continuum at 5100 Å were 1.5-10 days for the Balmer lines, and 0.0 -2.6 days for the HeII λ4686 line (Sergeev et al. 2001). Recently, Bentz et al. (2006) analyzed the observations performed between February 27 and April 10, 2005. They obtained a time lag for the Hβ line of $6.6^{+1.1}_{-0.8}$ days.

NGC 4151 was also monitored in the UV. Clavel et al. (1990) analyzed the spectra obtained with the IUE satellite during two months from November 29, 1988, to January 30, 1989 (with a ~4 days sampling time) and they found a time lag of 4 ± 3 days between the continuum and the lines CIVλ1549 and Mg IIλ2798. In addition, NGC 4151 was observed with IUE from November 9 to December 15, 1991 (35 days), with a one day sampling time (see Ulrich & Horne 1996). Ulrich & Horne (1996) found that the time delay in the continuum at 3000 Å with respect to that at 1320 Å was smaller than one day (i.e. the UV continuum is emitted by a region with a dimension less than one light day). The broad UV emission lines showed large variations that closely followed the continuum ones. For CIVλ1549, the time lag relative to the continuum was 2.4-3.8 days. Ulrich & Horne (1996) observed also deep blue-shifted absorption lines. They are produced by a low-velocity gas which covers the major part of the rapidly varying continuum source and the emission-line regions. This material is moving outwards along the line of sight, and may be located anywhere beyond 15 lt-days. Kaspi et al. (1996) observed NGC 4151 during two months in 1993, with a time resolution of about one day. They found no evidence for any time lag between the optical and UV continuum, and a time lag of 0-2 days for Hα, and 0-3 days for Hβ. Recently, Metzroth et al. (2006) re-analyzed the IUE spectra of NGC 4151 obtained in 1988 (Clavel et al. 1990) and in 1991 (Ulrich & Horne 1996), using the New Spectral Image Processing System (NEWSIPS). This allowed to improve the photometric precision and to increase the S/N ratio by 10%-50%. They found that the time lags of the revised responses to changes of the continuum were ~ 3-7 days for CIVλ1549, HeIIλ1640, CIII]λ1909, and MgIIλ2798.

The results mentioned above indicate that the dimension of the BLR varies among the emission lines (radial stratification) and is changing with time. Contradictory results have been obtained, even for the same species, after using the modified processing system and re-analyzing old data (for instance, Antonucci & Cohen 1983, Gaskell & Sparke 1986, Peterson & Cota 1988, Ulrich & Horne 1996, Metzroth et al. 2006). Inconsistent time lags from different monitoring campaigns might be caused by the short duration of the campaigns, but might also indicate real changes in the BLR size and geome-

try. E.g., Lyuty (2005) analyzed photometric observations performed during more than 30 years, and concluded that the NGC 4151 nucleus goes through different levels of activity. They could be related to a total destruction of the accretion disk (AD) that took place in cycle A (from 1968 to 1984), and the formation of a new AD in cycle B (from 1989 to 1996). Nevertheless, most UV and optical monitoring campaigns confirmed that the BLR is small and is radially stratified.

Unfortunately, spectral optical monitoring of NGC 4151 were mostly carried out during short periods (less than one year), which are insufficient to trace real changes in the BLR structure. In order to study the evolution of the BLR, more than 10 years of spectral monitoring is needed. Such observations have been **made** since 1986 in CrAO (Malkov et al. 1997; Sergeev et al. 2001) and SAO RAS (Bochkarev et al. 1988, 1991; Shapovalova et al. 1996; Nazarova et al. 1998).

In this paper we present the analysis of the spectral monitoring of NGC 4151 that covers a 11-years period from 1996 to 2006. The paper is organized as follows: in §2 the observations, data reduction and calibration are explained. In §3 we study the correlations between the continuum, the Balmer (Hα, Hβ, Hγ) and the HeIIλ4686 fluxes, for both the whole lines and the line wings. In §4 we discuss different possible interpretations. The results are summarized in §5.

2. Observations and data reduction

2.1. Optical Spectroscopy

Spectroscopic observations of NGC 4151 were carried out between January 11, 1996 (Julian Date = JD 2450094) and April 20, 2006 (JD 2453846), thus covering a period of more than 10 years. In total 180 blue and 137 red spectra were taken during 220 nights, with the 6-m and 1-m telescopes of SAO, Russia (1996–2006), with the 2.1-m telescope of the Guillermo Haro Astrophysical Observatory (GHAO) at Cananea, Sonora, México (1998–2006), and with the 2.1-m telescope of the Observatorio Astronómico Nacinal at San Pedro Martir (OAN-SMP), Baja California, México (2005–2006). The spectra were obtained with a long–slit spectrograph equipped with CCDs. The typical wavelength range was 4000 - 7500 Å, the spectral resolution was R=5–15 Å, and the S/N ratio was > 50 in the continuum near Hα and Hβ. Note that from 2004 to 2006, the spectral observations with the GHAO's 2.1-m telescope were carried out with two variants of the equipment: 1) with a grism of 150 l/mm (a low dispersion of R=15 Å, like the observations of 1998–2003); 2) with a grism of 300 l/mm (a moderate dispersion of R=7.5Å). As a rule, the observations were performed with the moderate dispersion in the blue or red bands during the first night of each set; usually during the next night we used the low dispersion in the whole range 4000-7500 Å; the moderate dispersion was used in the following night. Since the shape of the continuum of active galaxies practically does not change during adjacent nights, it was easy to link together the blue and red bands obtained with the moderate dispersion, using the data obtained for the continuum with the low-dispersion in the whole wavelength range. The photometric accuracy is thus considerably improved with respect to a link obtained by overlapping the extremities of the continuum (3-5% instead of 5-10%).

Spectrophotometric standard stars were observed every night. Informations on the source of spectroscopic observations are listed in Table 1. Log of the spectroscopic observations is given in Table 2 (available only in electronic form).

Table 1. Sources of spectroscopic observations: 1 - source (Observatory); 2 - code assigned to each combination of telescope+equipment and used throughout this paper; 3 - telescope aperture and the spectrograph; 4 - projected spectrograph entrance apertures (the first number is the slit width, and the second is the slit length); 5 - focus of the telescope.

Source	Code	Tel.and Equip.	Aperture (arcsec)	Focus
1	2	3	4	5
SAO(Russia)	L(N)	6m+Long slit	2.0×6.0	Nasmith
SAO(Russia)	L(U)	6m+UAGS	2.0×6.0	Prime
SAO(Russia)	L(S)	6m+Scorpio	1.0×6.0	Prime
Gullermo Haro(México)	GH	2.1m+B&C	2.5×6.0	Cassegrain
San–Pedro(México)	S-P	2.1m+B&C	2.5×6.0	Cassegrain
SAO(Russia)	L1(G)	1m+GAD	4.2(8.0)×19.8	Cassegrain
SAO(Russia)	L1(U)	1m+UAGS+CCD2K	4.0×9.45	Cassegrain

The spectrophotometric data reduction was carried out either with the software developed at the SAO RAS by Vlasyuk (1993), or with IRAF for the spectra observed in México. The image reduction process included bias subtraction, flat-field corrections, cosmic ray removal, 2D wavelength linearization, sky spectrum subtraction, addition of the spectra for every night, and **relative flux calibration** based on standard star observations.

2.2. Absolute calibration and measurements of the spectra

The standard technique of flux calibration spectra (i.e. comparison with stars of known spectral energy distribution) is not precise enough for the study of AGN variability, since even under good photometric conditions, the accuracy of spectrophotometry is not better than 10%. Therefore we used standard stars only for a relative calibration.

For the absolute calibration, the fluxes of the narrow emission lines are adopted for scaling the AGN spectra, because they are known to remain constant on time scales of tens of years (Peterson 1993). We thus assume that the flux of the [O III]λ5007 line was constant during the monitoring period. One can indeed check that it did not change between 1980 (Antonucci & Cohen 1983) and 1992 (Malkov et al. 1997). This is due to the fact that the forbidden line emitting region is very extensive (more than a hundred light-years). All blue spectra were thus scaled to the constant flux $F([O III]\lambda 5007) = 1.14 \times 10^{-11}$ erg s^{-1} cm^{-2} determined by Malkov et al. (1997), and corrected for the position angle (PA), seeing and aperture effects, as described in §2.3. The scaling of the blue spectra was performed by using the method of Van Groningen & Wanders (1992) modified by Shapovalova et al. (2004)[1]. This method allowed us to obtain a homogeneous set of spectra with the same wavelength calibration and the same [OIII]λ5007 flux.

The spectra obtained using the GHAO 2.1–m telescope (México) with a resolution of 15 Å contain both the Hα and Hβ regions. These spectra were scaled using the [O III]λ5007 line. In this case the red region was automatically scaled also by the [O III]λ5007 flux. However, the accuracy of such a scaling depends strongly on the correct determination of the continuum slope within the whole wavelength range (4000-7500), i.e. on a correct correction for the spectral sensitivity of the equipment, which is determined by a comparison star. If the night of the observation had not good photometric conditions (clouds, mist, etc.), the reduction can give a wrong **spectral** slope and, consequently, the errors in scaling the Hα wavelength band can be large. Most of the spectra from the 1-m and 6-m SAO telescopes

were obtained separately in the blue (Hβ) and in the red (Hα) bands, with a resolution of 8 – 9 Å. Usually, the red edge of the blue spectra and the blue edge of the red spectra overlapped within an interval of $\sim$ 300 Å. Therefore, as a zero approximation (the first stage) the majority of red spectra was scaled using the overlapping continuum region with the blue spectra, which were scaled with the [O III]λ5007 line. In this case the scaling uncertainty is about 5%-10%. However, for some red spectra, this method could not be used because some spectra obtained with a higher resolution ($\sim$ 5Å) did not overlap with blue spectra; or some spectrum ends were distorted by the reduction procedures of the instrumental set-up; or the blue and red spectra were not taken during the same night. Therefore, to increase the precision of the Hα spectral region (the second stage), all red spectra were **once more** scaled to a constant flux value of the narrow emission line [OI]λ6300, using the modified method of Van Groningen & Wanders (1992, see also Shapovalova et al. 2004). As a reference, we used a red spectrum obtained with the GHAO 2.1-m telescope during a good photometric night, and well-scaled by the [OIII]λ5007 line. **After scaling all red spectra using the [OI]λ6300 Å line, we were able to estimate the quality of each spectrum by comparing the [OI] and the [OIII] scalings, and we eliminated the low quality spectra in the further analysis.** The uncertainty of the scaling of red spectra by the line [OI]λ6300 (i.e. actually by the flux of the [OIII]λ5007 line) was then about (2-3)%.

Then from the scaled spectra we determined an average flux in the continuum at the observed wavelength $\sim$ 5117 Å (i.e. at $\sim$ 5100 Å in the rest frame of NGC 4151, z=0.0033), by averaging the fluxes in the band 5092 – 5142 Å. To determine the observed Hβ and Hα fluxes, it is necessary to subtract the continuum. **The continuum was estimated in 30 Å windows, and was fitted by a straight line between two windows centred respectively at 4590 Å and 5125 Å for Hβ, and at 6200 Å and 6830 Å for Hα.** After subtracting the continuum, we measured the observed fluxes in the lines, in the following wavelength intervals: 4780 – 4950 Å for the Hβ, and 6415 – 6716 Å for Hα.

To measure the fluxes of Hγ and HeIIλ4686, we used only 115 blue spectra from a total of 180. The **remaining** 65 blue spectra were not suitable, because they begin at $\lambda > 4300$ Å, or had a bad correction for spectral **sensitivity** at the edge of the blue region (for example, because of bad weather). The underlying continuum for Hγ and HeII λ4686 was fitted by a straight line using estimates of the continuum in a 30 Å window centered respectively at 4230 Å and 5125 Å. After continuum subtraction, the Hγ and HeIIλ4686 fluxes were measured in the fol-

---

[1] see Appendix A in Shapovalova et al. (2004)

lowing wavelength intervals: 4268 – 4450 Å for Hγ, and 4607 – 4783 Å for HeII λ4686.

2.3. Correction for the position angle (PA), seeing and aperture effects

In order to investigate the long term spectral variability of NGC 4151, it is necessary to have a consistent set of spectra. Since NGC 4151 was observed with different telescopes, in different position angles, and with different apertures, first we had to perform corrections for the position angle (PA), seeing and aperture effects. A detailed discussion on the necessity for these corrections is given in Peterson et al. (1995), and will not be repeated here.

2.3.1. Correction for the position angle (PA) effect

The position angle corresponds to the position of the slit of the spectrograph on the sky (from the North to the East direction). Usually, the observations were performed with PA=90°, but sometimes it was not possible, e.g. at the 6m - Nesmith focus, etc. Note that the atmospheric dispersion was very small, since the object was always observed close to the meridian ($< 2h$ and $z < 30°$). To make the correction for the position angle, 80 spectra of NGC 4151 were taken with the 1-m and 6-m SAO telescopes on May 8 and 9, 2003, under photometric conditions and a good seeing (1.2"-1.5"), in different position angles (PA=0, 45, 90, 135 degrees), and with different spectrograph entrance slits (1", 1.5", 2", 4", 8"). Data sets with PA=90 degrees for different slits were used as standard, since most of NGC 4151 spectra in our monitoring campaign were obtained in this position angle. Then we determined corrections for the PA effect $k(pa)$, as:

$$k(pa) = F(90)/F(i),$$

where $F(i)$ is the observed flux at PA=i degrees, and $F(90)$ is the flux obtained at PA=90 degrees. In Table 3 (available only in electronic form), we list the PA corrections $k(pa)$ for the Hβ and continuum fluxes, obtained for PA=0, 45, and 135 degrees, with apertures 2.0"×6.0" and 4"×20.25". As can be seen from Table 3, the variations of $k(pa)$ between the Hβ and continuum fluxes in the same PA is small (<1%), except for PA=45 degrees where they are <3%. A maximum PA correction for the continuum flux, $kp(cnt)=1.1$, was obtained with PA=45 degrees and an aperture 2"×6.0". This PA nearly corresponds to the axis of the ionized cone (PA~50 degrees). The line and continuum fluxes were determined for PA=90 degrees, using a linear interpolation of the $k(pa)$ values of Table 3.

2.3.2. Correction for the seeing effect

The Narrow Line Region (NLR) of NGC 4151 has an extended bi-conical structure spreading up to >2" from the nucleus (Evans et al. 1993), while the BLR and non-stellar (AGN) continuum are effectively point-like sources ($\ll 1''$). Consequently, the measured NLR flux depends on the size of the spectrograph entrance aperture (see Peterson et al. 1995 for a detailed discussion). Also, since we observed with different telescopes and apertures, for each aperture the measured ratio of the BLR flux (a point-like source) to the NLR flux (a spatially extended region) depends on the seeing. Therefore, in each aperture we must find corrections for images and reduce all flux data to some accepted standard image. The method suggested by Peterson et al. (1995)

has been used for this purpose. For the seeing in each aperture we can write:

$$F(s) = k(s) \cdot F(pa) - G(s)$$

where $F(pa)$ is the observed flux at PA=90 degrees, $F(s)$ is the seeing corrected flux, $k(s)$ is a point-source correction factor, and $G(s)$ is an extended source correction taking into account the host galaxy light. Obviously, $G(s) = 0$ for the broad-line flux (point-like source).

We have divided the whole range of seeing values into several intervals, for two different apertures. For the first aperture, 2.0"(2.5")×6.0", which corresponds to the observations with the 6-m and 2.1-m telescopes (México), we considered the following intervals: 1"-1.5"; 1.5"-2.5"; 2.5"-3.5"; 3.5"-4.5"; and >4.5". The data set for the interval 1.5"-2.5" was adopted as a standard one since the average seeing in the period of observations with this aperture was about 2". A value $k(s) =1$ and $G(s)=0$ was accepted for this standard data set. We obtained the seeing correction $k(s)$ and the extended source correction $G(s)$ for the seeing intervals mentioned above using spectra observed with different seeings within a time interval shorter than 3 days (i.e. $k(s) = F(1.5" − 2.5")/F(pa)_i$, where $F(pa)_i$ is the observed flux in PA=90 for the i-seeing, and $F(1.5" − 2.5")$ is the flux for the seeing interval 1.5"-2.5"; these data are separated by 3 days or less). In Table 4 (available only in electronic form) we listed the $k(s)$ and $G(s)$ corrections and the data obtained from Peterson et al. (1995, their Figs. 5 and 6) for the aperture 2"×10". From this table, one can see that our seeing corrections $k(s)$ for an aperture of 2"×6" practically coincide (within 1%) with those of Peterson et al. (1995) for an aperture of 2"×10". **The correction ($k(s)$ in Table 4) for the emission line fluxes is the same for a slit length of $6''$ and of $10''$, meaning that the lines are emitted by a region smaller than $6''$, but there are significant differences in the host galaxy contribution, as expected.**

For the second aperture, 4.2"×19.8", which corresponds to our observations with the 1-m Zeiss telescope (SAO), we used the seeing intervals 2"-4", 4"-6", 6"-8". They are large because with this telescope it is impossible to determine the seeing quality with a good precision, owing to the small scale along the spectrograph slit (2.2"/px). The data set for the interval 2"- 4" was used as a standard. The seeing corrections $k(s)$ and $G(s)$ for the aperture 4.2"×19.8" were obtained with the same procedure described above for the aperture 2"×6". The results are given in Table 5 (available only in electronic form), together with those of Peterson et al. (1995) for the aperture 5"×7.5" (their Figs. 5 and 6).

Emission line and continuum fluxes were scaled to the mean seeing 2" for the apertures 2"×6.0"(2.5"×6.0"), and to the mean seeing 3" for the aperture 4.2"×19.8", using the seeing corrections from Tables 4 and 5. **After that, we scaled all spectra to the 2"×6.0" aperture (cf. below).**

2.3.3. Correction for the aperture effect

To correct the observed fluxes for aperture effects, we determined a point-source correction factor φ using the equation (see Peterson et al. 1995 for a detailed discussion):

$$F(Hb)true = \varphi \cdot F(Hb)obs,$$

where $F(Hb)obs$ is the observed Hβ flux after correction for the PA and seeing effects, as described in §2.3.1 and §2.3.2; $F(Hb)true$ is the Hβ flux corrected for the aperture effect.

Table 6. Flux scale factors for optical spectra

Sample	Years	Aperture (arcsec)	Point-Source Scale factor (φ)	Extended Source Correction $G(g)^a$
L(U,N)	1996-2005	2.0×6.0	1.000	0.000
GH,S-P	1996-2005	2.5×6.0	1.000	0.000
L(S)	2004-2006	1.0×6.0	0.950±0.000	-0.391
L1(G)	1996-2003	4.2×19.8	1.035±0.021	1.133±0.037
L1(G)	1996-2003	8.0×19.8	1.112±0.005	1.623±0.080
L1(U)	2004-2006	4.0×9.45	0.962±0.044	0.750±0.150

^{a} in units $10^{-14} (\mathrm{erg\,s^{-1}\,cm^{-2}\,\text{Å}^{-1}})$

The contribution of the host galaxy to the continuum flux depends also on the aperture size. The continuum fluxes $F_\lambda(5117)$ were corrected for different amounts of host-galaxy contamination, according to the following expression (see Peterson et al. 1995):

$$F(5117\text{Å})true = \varphi \cdot F(5117\text{Å})obs - G(g),$$

where $F(5117A)obs$ is the observed continuum flux after correction for the PA and seeing effects, as described in §2.3.1 and §2.3.2; $G(g)$ is an aperture – dependent correction factor to account for the host galaxy contribution. The cases L (Table 1), which correspond to the aperture ($2'' \times 6''$) of the 6-m telescope, was taken as a standard (i.e. $\varphi = 1.0$, $G(g)=0$ by definition). The corrections φ and $G(g)$ were defined for each aperture via the comparison of a pair of observations separated by 0 to 2 days. It means that the variability on shorter times (< 2 days) was suppressed by the procedure of data re-calibration. The point-source correction factors φ and $G(g)$ values for various samples are given in Table 6. Using these factors, we re-calibrated the observed fluxes of Hα, Hβ, Hγ and HeIIλ4686 and of the continuum to a common scale corresponding to the aperture $2'' \times 6''$ (Table 7 -available only in electronic form).

The fluxes listed in Table 7 were not corrected for contamination by the narrow-line emission components of Hγ, HeIIλ4686, Hβ, Hα, and [N II]λλ 6548, 6584. These contributions are expected to be constant and to have no influence on the broad line variability.

The mean error (uncertainty) in our flux determinations for Hα and Hβ and for the continuum is <3%, while it is ∼ 5% for Hγ and ∼ 8% for HeII λ4686. These quantities were estimated by comparing the results from spectra obtained within time intervals shorter than 2 days. The estimated mean errors for every year and for the total period of monitoring are given in Table 8 (available only in electronic form).

2.4. The narrow emission line contribution

In order to estimate the narrow line contributions to the broad line fluxes, we constructed a spectral template for the narrow lines. To this end, we used the blue and red spectra in the minimum activity state (May 12, 2005), obtained with a spectral resolution of ∼ 8 Å. In these spectra, the broad Hβ component was very weak, and the broad components from the higher Balmer line series were absent.

Both the broad and the narrow components of Hγ, HeIIλ4686, Hβ and Hα, were fitted by Gaussians. The template spectrum contains the following lines: for Hγ: the narrow component of Hγ and [O III]λ 4363; for Hβ: the narrow component

Table 9. The wavelength integration intervals and the corresponding NLR contributions

Components	integration intervals (Å)	NLR flux^a
Hα+[NII]	6415-6716	7.93
Hβ-nar.	4780-4950	1.00
Hγ+[OIII]λ4363	4268-4450	1.04
HeII+[ArIV]+ [FeIII] 4658	4607-4783	0.36

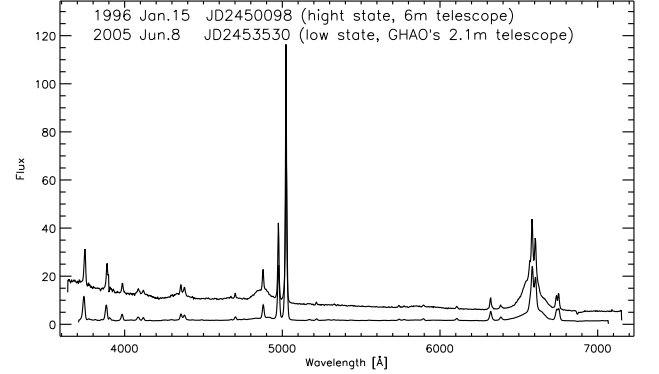^{a} in 10^{-12} erg cm^{-2} sec^{-1}

Fig. 1. The spectra of NGC 4151 corresponding to the high activity state (top) and to the low activity state (bottom). The observed wavelength (we recall that z=0.0033) is displayed on the X-axis, and the flux (in units of 10^{-14} erg cm^{-2} s^{-1} Å^{-1}) is displayed on the Y-axis.

of Hβ and [O III]λλ 4959, 5007; for Hα: the narrow component of Hα, [N II]λλ 6548, 6584, [O I]λλ 6300, 6364,) [S II]λλ 6717, 6731 and HeI λ 6678. In Table 9 are listed the narrow line contributions obtained from the template spectrum in the same wavelength integration intervals as for integral fluxes. Our results are in good agreement with those given by Sergeev et al. (2001).

3. Data analysis

3.1. Variability of the emission lines and of the optical continuum

The spectra for the high- and low-activity states, obtained respectively on January 15, 1996 (6m SAO's telescope) and on June 8, 2005 (2.1 m GHAO's telescope) are presented in Fig. 1. As can be seen, the continuum flux decreased by a large factor (∼ 5.6 times) in the low-activity state, and the slope of the continuum in the blue was significantly flatter than in the high-activity state. Besides, the wings of Hβ and Hα became extremely weak in the minimum state, and those of Hγ and of the higher Balmer line series could not be detected at all. These profiles correspond to a Sy 1.8 type and not to a Sy1-Sy1.5, as this AGN could be classified in the maximum state. So, the spectral type of the object is changing with time. This was noted earlier. In 1984-1989, the nucleus of NGC 4151 went through a very deep minimum. At that time, the brightness of the source fell down to the level of the host galaxy for an aperture of 27" in the V-band, the broad wings of hydrogen lines became much weaker (they almost completely vanished in April 1984) and the spec-
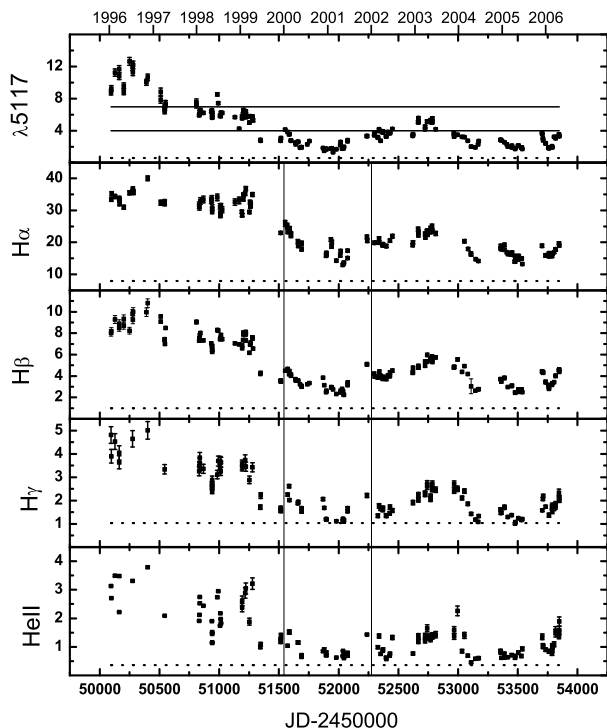
Fig. 2. The light curves of Hα, Hβ, Hγ, HeIIλ4686 and of the continuum at the observed wavelength λ =5117 Å, in the period 1996-2006. Constant contributions from the narrow lines (Table 9) and from of the host galaxy (see 3.1) are shown by horizontal dashed lines. The line fluxes are given in units of 10^{-12}erg cm^{-2}s^{-1}, and the continuum flux in units of 10^{-14}erg cm^{-2}s^{-1}Å^{-1}. **The horizontal lines in the first panel correspond to the division of the continuum flux into three intervals (see §3.4.2), and the vertical lines correspond to the division into time intervals based on the similarity of the line shapes (see §3.3).**

trum of the nucleus was identified as a Sy 2 (Penston & Perez 1984).

In Fig. 2 are presented the light curves obtained from Table 7, for the Hα, Hβ, Hγ and HeIIλ4686 integrated line fluxes and for the continuum at the observed wavelength 5117Å. The fluxes of Hγ, HeIIλ 4686, Hβ, and Hα were not corrected for contamination by the constant contributions of the narrow lines. The contributions of the narrow lines given in Table 9 are shown in Fig. 2 by horizontal dashed lines. It is clearly seen that if the fluxes of the narrow lines are subtracted from Hγ and HeIIλ 4686 during the minimum of activity, these lines disappear.

The continuum flux presented in Table 7 and in Fig. 2 contains also a constant contribution from the starlight of the host galaxy, which is estimated as F(host) = 1.54 10^{-14}erg cm^{-2}s^{-1}Å^{-1} through an aperture of 5"×7.5"

Table 10. Mean observed maximum flux F_{obs}^{max} in the intervals JD=2450094-2450402 (1996), mean observed min flux F_{obs}^{min} in the intervals JD=2451895-2452043 (December 2000 - May 2001) and 2453416-2453538 (2005), observed ratio R_F =F_{obs}^{max}/F_{obs}^{min}, and this ratio for the broad lines (R_F^{broad}) after removing the narrow components and the contribution of the host galaxy.

Lines or continuum[a]	F_{obs}^{max}	F_{obs}^{min}	R_F	R_F^{broad}
Hα	34.860	15.340	2.3	3.6
Hβ	9.170	2.640	3.5	5.0
Hγ	4.365	1.178	3.7	24!(not broad)
HeIIλ4686	3.170	0.714	4.4	7.9
cont(5117A)	10.69	1.9	5.6	7.8 agn continuum

[a] Line fluxes are in units 10^{-12}erg cm^{-2}s^{-1}; and continuum flux is in units 10^{-14}erg cm^{-2}s^{-1}Å^{-1}

(Peterson & Cota 1988), and 10^{-14}erg cm^{-2}sec^{-1}Å^{-1} through an aperture of 3"×10" (Mal'kov et al. 1997). Bochkarev et al. (1991) determined that the host galaxy contributed to about 40% of the total flux of NGC 4151 in the Hβ wavelength band though an aperture 1"×4.0", near the minimum state (1987). As can be seen from Table 7, the minimum flux in the continuum (~ 1.6 10^{-14}erg cm^{-2}s^{-1}Å^{-1}) obtained with an aperture 2"×6" was observed from November 29 to December 17, 2000. If we assume that the host galaxy contribution is about 40% of the continuum (Bochkarev et al., 1991), it gives F(host) > 0.6 10^{-14}erg cm^{-2}s^{-1}Å^{-1} (i.e. lower limit). Using a linear regression between the continuum flux and the Hα and Hβ broad line fluxes (the narrow line flux being subtracted) near the low-activity state, and extrapolating the broad line flux to zero, we estimated F(host)≈ (0.6±0.3)x10^{-14}erg cm^{-2}s^{-1}Å^{-1}. This value is in good agreement with other estimates with different apertures. The estimated contribution from the host galaxy is shown by the horizontal dashed line in Fig. 2 (top).

The light curve of the continuum is similar to those of the emission lines, showing a maximum in 1996 and two minima in 2001 and 2005.

In Table 10, we give for the lines and continuum, the mean observed maximum flux F(max) in the interval JD=2450094-2450402 (1996), the mean observed minimum flux F(min) in the intervals JD=2451895-2452043 (December 2000 - May 2001), and JD=2453416-2453538 (2005), the observed ratio F(max)/F(min), and this ratio for the broad lines after subtraction of the narrow components and the contribution of the host galaxy (agn continuum in Table 10).

The maximum amplitude ratios of the broad component line flux during the 1996-2006 period were: ~ 3.6 for Hα; ~ 5.0 for Hβ line; and ~ 7.8 for the λ5117 Å agn continuum after subtraction of the host galaxy flux. In the low-activity state, the broad component of HeIIλ4686 and Hγ was almost absent.

3.2. Flux variability in the wings and core of the Hα and Hβ emission lines

We have divided the Hα and Hβ profiles into three parts: the blue wing, the core, and the red wing, each part covering a range of 3000 km/s. Distinct features or peaks observed at different epochs in the wings were included, and the corresponding narrow lines were included in the core. In Table 11, we give the
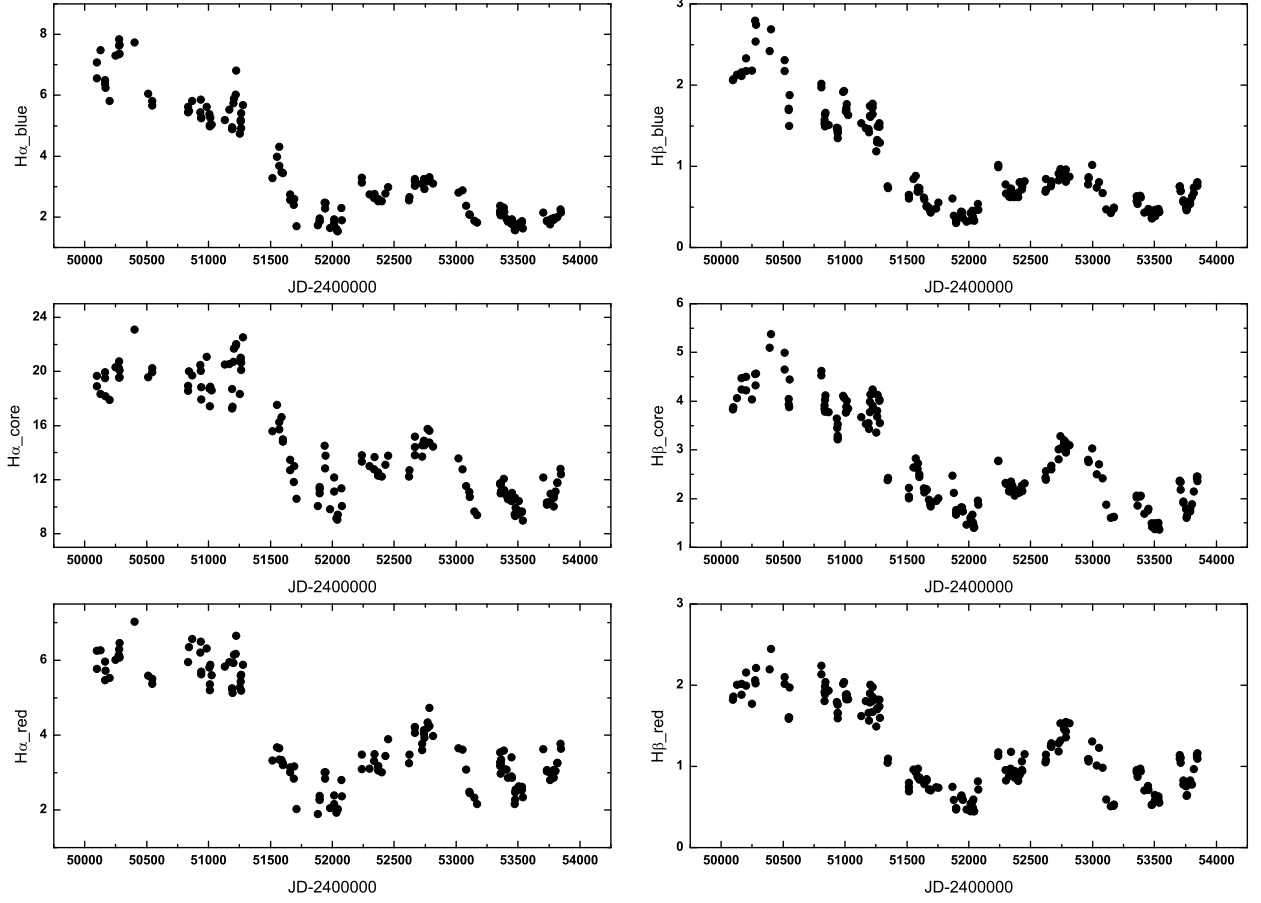
Fig. 3. The variation of the wings and core of Hα (left) and Hβ (right) from 1996 to 2006. The flux is given in units of 10^{-12}erg cm^{-2}s^{-1}.

Table 11. The wavelength intervals for the Hα and Hβ wings and cores.

Component	Integration interval in Å	Integration interval in km/s
Hα blue wing	6486-6552	(-4510) - (-1503)
Hα core	6553-6616	(-1458) - (+1402)
Hα red wing	6617-6684	(+1458) - (+4510)
Hβ blue wing	4804-4853	(-4493) - (-1479)
Hβ core	4854-4900	(-1417) - (+1412)
Hβ red wing	4901-4950	(+1474) - (+4488)

wavelength intervals used to measure the flux in the three parts of each profile. We also give the corresponding velocity intervals with respect to the center of the narrow component.

Light curves for the wings and cores of Hα and Hβ are presented in Fig. 3. As it can be seen, the flux in the wings and cores of both lines had a very similar behaviour during the monitoring period.

In Fig. 4 we present the flux ratios between the three parts of the Hα and Hβ profiles. In both lines, the blue wing had a stronger flux than the red one in the period of maximal activity (March 1996 to 1997 or JD=2450094-2450500) (F(blue)/F(red)>1, see Fig. 4, top-left). From 1997 to 2000 (or JD=2450540-2451500), the Hα blue/red flux ratio was very close to unity, while the Hβ blue/red ratio varied from 0.95 to 0.8 (Fig. 4, top-right). In 2000-2006 (JD=2451550-2453850), the red wing was the strongest for both lines, and the Hα blue/red ratio decreased almost monotonically from 0.8 to 0.6 (Fig. 4, top-left), while it varied from 0.6 to 0.8 for Hβ (Fig. 4, top-right).

The F(blue)/F(core) ratio of both lines was decreasing nearly monotonically from 1996 to 2001 (JD=2450094-2452000), and after 2002 (JD>2452300), the Hβ ratio remained nearly constant (≈ 0.3), while the Hα ratio decreased very slightly (Fig. 4, middle). On the other hand, the F(red)/F(core) ratio of both lines showed approximaly the same rapid changes in the monitoring period.
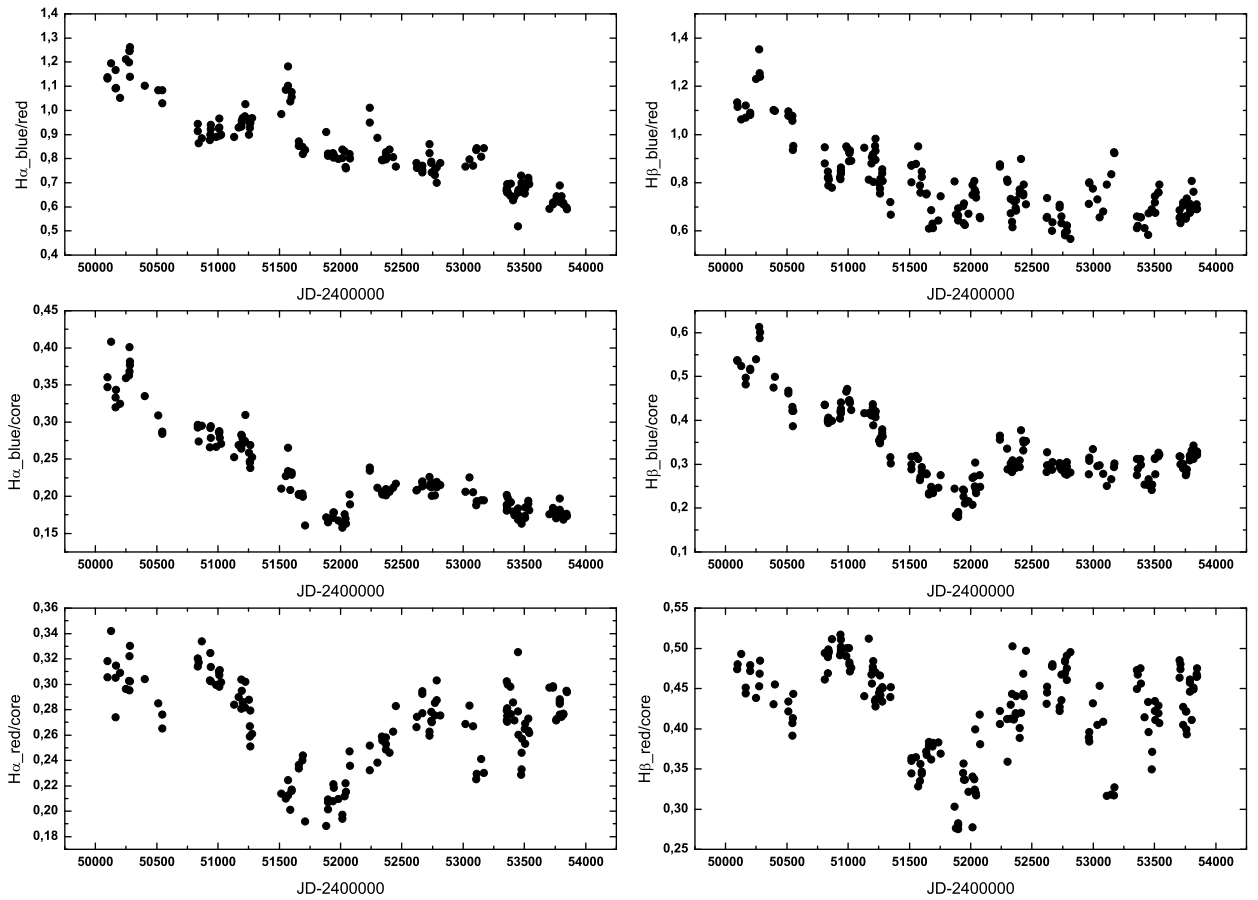
Fig. 4. The variation of the ratio of the fluxes in the line wings and in the core of Hα (left) and Hβ (right) (see the text), from 1996 to 2006.

Fig. 5. The averaged and rms profiles of **the broad** Hα (left) and Hβ (right) **lines** for the first period.
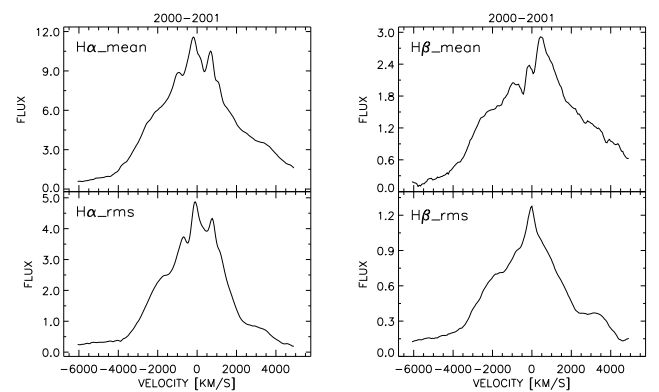
Fig. 6. The averaged and rms profiles of **the broad** Hα (left) and Hβ (right) **lines** for the second period.

3.3. Mean and Root-Mean-Square Spectra

The comparison between the averaged and the root-mean-square (rms) spectra allows to investigate the line profile variability. We first made an inspection of the Hα and Hβ profiles for dif-

ferent periods, using spectra with a resolution of 8 Å. With a criteria based on the similarity of line profiles, we found three characteristic profiles during the period 1996-2006. In the first period (1996-1999, JD=(2450094.466-2451515.583), where the

lines were very intense, a red asymmetry and a shoulder in the blue wing were present. In the second period (2000-2001, JD=2451552.607-2452238.000), the broad lines were weaker and the shoulder in the blue wing is smaller and a shoulder in the red part is present. From 2002 to 2006 (third period, JD=2452299.374-2453846.403), the lines showed a blue asymmetry, and a shoulder in the red part **was dominant in the line profiles** (peak at $\lambda \approx 4915$Å or at ≈ 2000 km/s relative to the narrow component, see Figs. 5-7, top).

Averaged and rms profiles of Hβ and Hα for each of these three periods and for the whole monitoring period (1996-2006) were calculated after removing the continuum. They are shown in Figs. 5-8.

We measured the Full Width at Half Maximum (FWHM) in the rms and averaged broad line profiles, and we defined the asymmetry A as the ratio of the red/blue Half Width at Half Maximum (HWHM), i.e. $A = HWHM_{\mathrm{red}}/HWHM_{\mathrm{blue}}$. The measured values for the broad Hβ and Hα lines and their rms are given in Table 12.

As can be seen in Fig. 5 (bottom), the blue component was highly variable in the first period, the rms profile of Hα and in a lesser extent of Hβ, showing two peaks or shoulders at ~ -4000 km/s and ~ -2000 km/s. In the red part of the rms profile of Hα, a weak bump at $+2000$ km/s and a shoulder at $+3500$ km/s was also detected, while in the rms profile of Hβ, only weak shoulders were seen at the same places. **On the other hand, the line and their rms profiles show a blue asymmetry ($A < 1$, see Table 12).** In the second period (see Fig. 6, bottom), the feature at ~ -4000 km/s in the blue part of the rms profile of both lines disappeared, and only a shoulder at ~ -2000 km/s was present. **The averaged Hα profile has a blue asymmetry, but the Hβ one is almost symmetric.** In the red part of the rms profile of both lines, the shoulder seen in the first period at ~ 3500 km/s was still present. This feature, but shifted at 2500 km/s, was dominant in the third period (Fig. 7), not only in the rms profiles of Hα and Hβ, but also in their averaged profiles. **Both lines show a red asymmetry in this period, but it is interesting to note that the Hα rms profile shows a significant blue asymmetry ($A \approx 0.82$), while the Hβ rms profile has a significant red asymmetry ($A \approx 1.17$).** Averaged and rms profiles are given in Fig. 8 for the whole monitoring period from 1996 to 2006. As can be seen, two shoulders dominate the rms profiles: a blue one at $\sim$-2000 km/s and a red one at $\sim$1500 km/s. Also, the variation in the blue part is more important than in the red one, because the line intensities during the whole monitoring period are dominated by the first period, when the variation in the blue part was the most important and at the same time the lines were the most intense. **Table 12 shows also that for the whole monitoring period, the rms profiles of both lines have a significant blue asymmetry, and that the averaged and rms FWHM of Hβ are larger than those of Hα by about 1000 km/s.**

Such a behaviour of the rms profiles during the three periods indicate that the BLR of NGC 4151 has a complex structure and that its geometry may change in time. More informations about line profiles will be given in a forthcoming paper.

3.4. The line and continuum flux correlations

3.4.1. The line-line and continuum-line relationship

To find the line-line flux relationships we have plotted the fluxes of Hα, Hγ and Heλ4686 vs. the Hβ flux (Fig. 9). As expected, there is a linear relation between the Hβ flux and that of the other lines. The correlation coefficients between the Hβ flux and
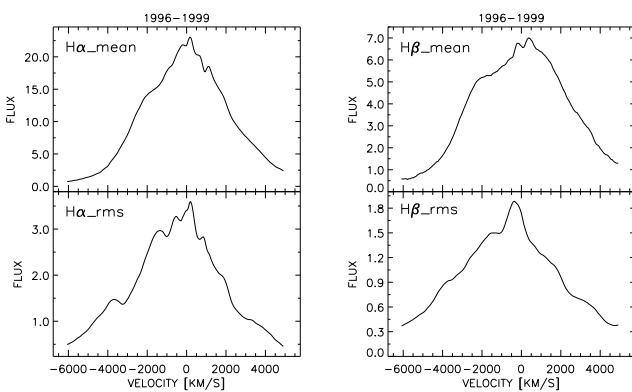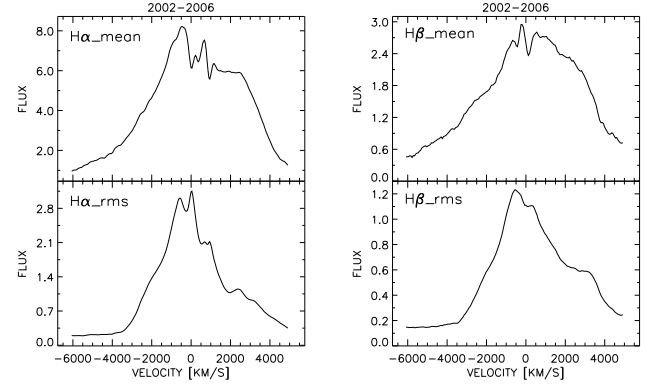

Fig. 7. The averaged and rms profiles of **the broad** Hα (left) and Hβ (right) **lines** for the third period.
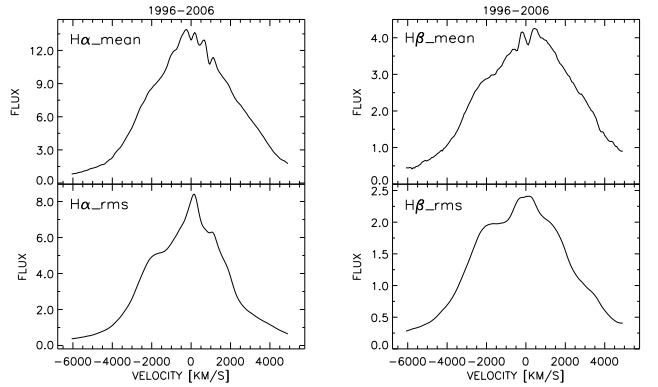
Fig. 8. The averaged and rms profiles of **the broad** Hα (left) and Hβ (right) **lines** for the whole monitoring period.

the Hα, Hγ and Heλ4686 fluxes are $r \approx 0.97$, 0.96 and 0.90, respectively. The slight differences between the correlation coefficients may be caused by uncertainty of the measurements (i.e. very weak Hγ and Heλ4686 in some periods)

We have also plotted the Hα, Hβ, Hγ and Heλ4686 fluxes against the continuum flux Fc (see Fig. 10). We find that the relationship between the line and continuum fluxes can be divided into two separated sequences. The first sequence, corresponding to $Fc \lesssim 7 \cdot 10^{-14}$erg cm^{-2}s^{-1}Å^{-1}, took place in the period 1998 to 2006; there was a linear relationship between the lines and continuum fluxes with a high correlation coefficient (0.88-0.95) for the Balmer lines. The behaviour of Heλ4686 vs. Fc is not clear, tending to be linear, but with a high dispersion ($r = 0.79$) when Fc was equal to $5.5-7$ 10^{-14} erg cm^{-2}s^{-1}Å^{-1}, corresponding to the period 1998-1999. The second sequence corresponds to large values of Fc ($\gtrsim 7$ 10^{-14} erg cm^{-2}s^{-1}Å^{-1}) and belongs to the period from 1996 to 1997. Here the line fluxes tended to remain constant, with a very weak correlation with Fc (see Fig. 10; $r \sim 0.2 - 0.48$ is given in the right-down corner for each line).

In Fig. 11 we show the relation between the continuum flux and the different parts of the Hα and Hβ profiles (the blue, the core, and the red). As can be seen, the relation for the core and the blue/red wing is similar to that of the whole line (see Fig. 10).

To find an explanation of this behaviour, we inspected these relationships within the three periods of observations mentioned

Table 12. The Full Widths at Half Maximum (FWHM) and the ratio $A = \text{HWHM}_{\text{red}}/\text{HWHM}_{\text{blue}}$ of the red/blue of Half Widths at Half Maximum (HWHM), for the averaged and rms profiles of Hα, Hβ during the three periods.

period	FWHM (Hα)	A_α	FWHM (Hβ)	A_β
first	4780±350	0.944±0.012	5980±550	0.935±0.048
second	4020±570	0.872±0.053	5550±750	1.086±0.067
third	5790±410	1.491±0.075	6350±430	1.282±0.112
mean profile	4650±420	1.000±0.023	6110±440	1.056±0.018
period	FWHM (rms Hα)	A_α - rms	FWHM (rms Hβ)	$A_\beta - rms$
first	4790±350	0.810±0.046	5430±530	0.596±0.017
second	3100±480	1.061±0.026	3700±550	0.811±0.068
third	3150±350	0.816±0.038	3760±1100	1.168±0.210
mean rms	4420±320	0.830±0.011	5490±420	0.775±0.023
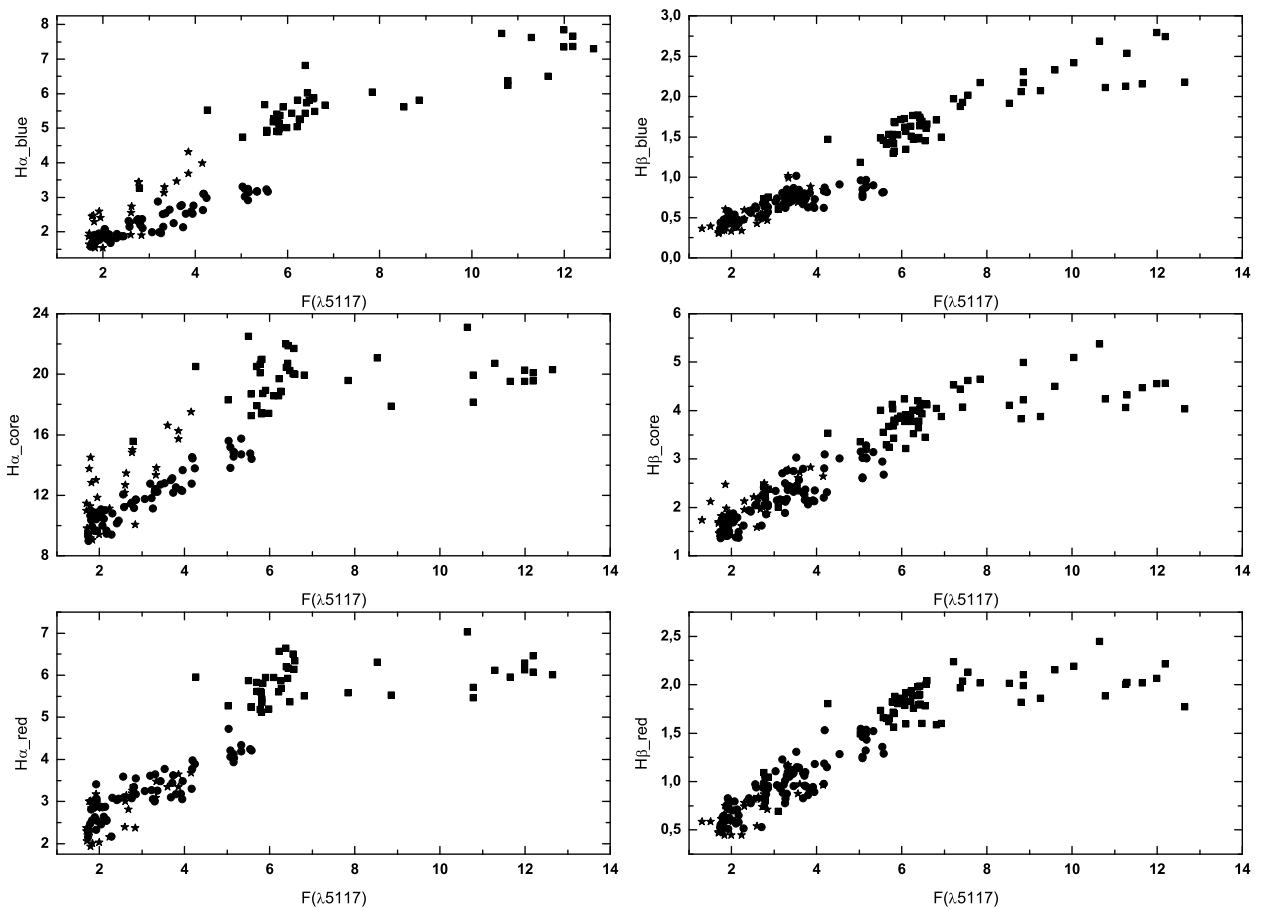
Fig. 11. The wings and core fluxes as a function of the continuum flux (at λ =5117 Å) for Hα (left) and Hβ (right). The line and continuum fluxes are given in the same units as in Fig. 10 .

above (see §3.3). We concluded that there was not only a difference in the line profiles, but also in the continuum vs. line flux relationships.

In the first period, when the lines were the most intense, there was a weak correlation between the lines and the continuum fluxes. The Hα flux changed by only ∼ ± 40%, while the continuum flux changed by a factor three (see Fig. 12, left).

During the same period, Hβ was also very weakly correlated to the continuum (Fig. 12, right), exept for five points, corresponding to observations between June and December 1999: at this time the continuum and Hβ fluxes decreased nearly by a factor two, but the Hβ and Hα profiles remained almost identical. In the second period, a large dispersion was observed for $Fc \lesssim 3.3 \cdot 10^{-14}$erg cm^{-2}s^{-1}Å^{-1}, and the lines did not respond to the con-
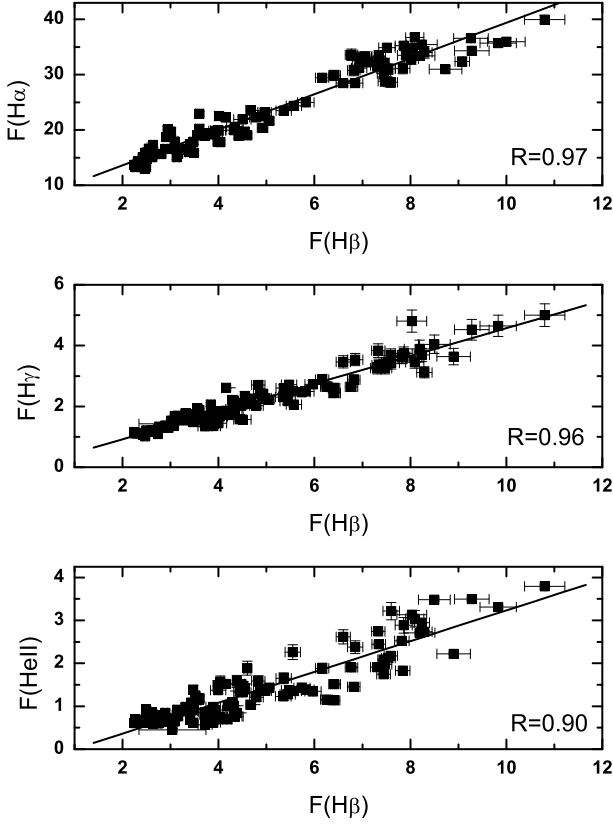
Fig. 9. The Hα, Hγ, HeIIλ4686 fluxes versus the Hβ flux. The correlation coefficients r are given inside the plot. The flux is given in units of 10^{-12}erg cm^{-2}s^{-1}.

Fig. 10. The Hα, Hβ, Hγ, HeIIλ4686 fluxes versus the continuum flux (at λ =5117 Å). The correlation coefficients r are given inside the plot. The line fluxes are given in units of 10^{-12}erg cm^{-2}s^{-1}, and the continuum flux in units of 10^{-14}erg cm^{-2}s^{-1}A^{-1}.

tinuum. Some points (5) with $Fc \geq 3.3\ 10^{-14}$ erg cm^{-2} s^{-1} Å^{-1} in Fig.12 (middle) correspond to spectra taken in January and February 2000, and their Hα and Hβ profiles are similar as in the first period (i.e. they have a red asymmetry and a shoulder in the blue wing). In the third period, the response of the lines to the continuum was linear.

3.4.2. Cross-correlation analysis

In order to determine the time lag between the optical continuum and the line variations (**line lagging continuum**), we used the **cross correlation function** – CCF method introduced by Alexander (1997), the Z-Transformed Discrete Correlation Function (ZDCF), which contains the idea of the Discrete Correlation Function (DCF) method (Edelson & Krolik 1988) avoiding an interpolation. The ZDCF approximates the bin distribution by a bi-normal distribution. This algorithm differs from the DCF in that the data points are equally binned, and it uses the Fisher's z-transform to stabilize a highly-skewed distribution of the correlation coefficient. According to Alexander (1997), ZDCF is much more efficient than DCF in detecting correlations involving the variability time-scale, and it is more sensitive to under-sampled light curves than DCF and Interpolated Cross-Correlation Function (Gaskell & Sparke 1986; Gaskell & Peterson, 1987).

The CCF analysis has been carried out for the full data set which covers the whole monitoring period from 1996 to 2006 and the three periods mentioned above. The time lags and CCF for Hβ and Hα are given in Table 13. As can be seen, the time lags for Hα and Hβ in the whole period are ~5 days, but they were different in the three periods. In the first and in the third period, the time lags were much smaller for both lines (from 0.6 to 1.1 days) than in the second period (11 and 21 days).

Moreover, we calculated the CCF and the time lags by dividing the data set into three groups according to the continuum intensity: (i) $F_{con}^1 \geq 7 \cdot 10^{-14}$erg cm^{-2}s^{-1}Å^{-1}; (ii) $F_{con}^1 > F_{con}^2 \geq 4 \cdot 10^{-14}$erg cm^{-2}s^{-1}Å^{-1} and (iii) $F_{con}^3 < F_{con}^2$. As it can be seen in Fig. 12, F_{con}^1 is only present during the first period, while F_{con}^2 and F_{con}^3 are present in all three periods. Table 13 shows that for such a division, the CCF is small when the continuum is high. Also, there is a big difference in the time lags between these three cases. Note that the highest CCF is obtained for the lowest continuum, but it is still smaller than the one obtained in the third period based on the line profiles.
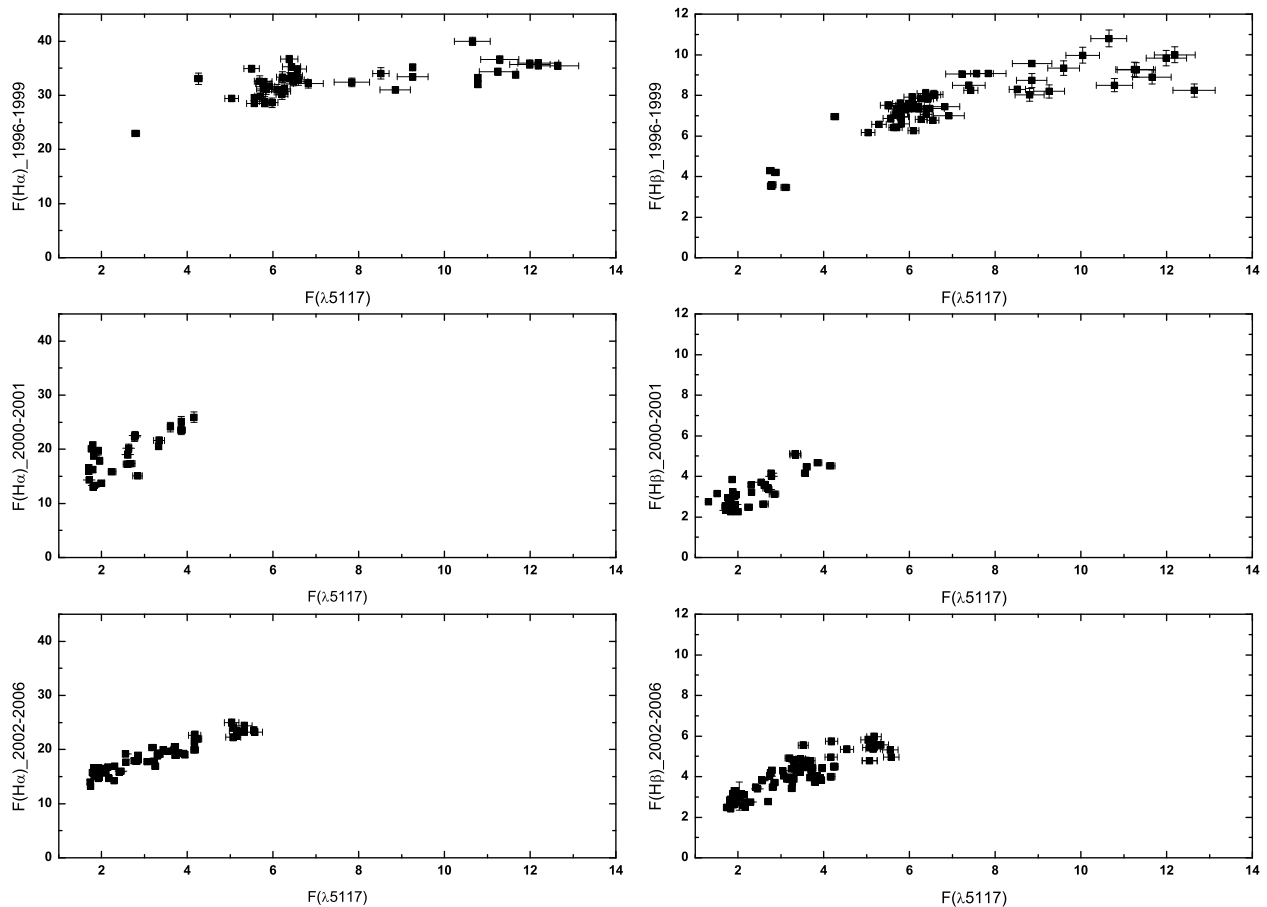
Fig. 12. Hα (left) and Hβ (right) fluxes for the three periods (first to third from top to down) as a function of the continuum flux. The line and conntinuum fluxes are given in the same units as in Fig. 10.

We can summarize the CCF analysis as follows. During the whole monitoring period, the time lags for the lines were: Hα – 5.70$^{+27.05}_{-5.70}$ days (CCF= 0.87$^{+0.02}_{-0.02}$); Hβ – 5.09$^{+27.89}_{-5.09}$ days (CCF 0.93$^{+0.01}_{-0.01}$). The large scatter of these values is due to the fact that the time lags were very different **for the three periods based on the profiles and also for periods based on the continuum intensity**.

To clarify these differences, we binned the observations using a time interval of three years starting from 1996, i.e. we calculated the time lags and CCFs for 1996-1997-1998, 1997-1998-1999, etc. The results are presented in Fig. 13, where the time lags (in light days) are given as a function of the central year of a three-year interval (e.g. for 1996-1997-1998, it is 1997). Full circles correspond to the maximal CCF values, and open circles correspond to CCF values consistent with the maximal values (i.e. within the error bars). By inspection of the CCF values and analysis of the results in Fig. 13, we found that there are always small lags corresponding to maximal CCF values or to CCF values consistent with the maximal ones. On the other hand, there are sometimes also large lags corresponding to maximal CCF values or to CCF

marginally consistent with these values. To summarize: a) in periods where the CCF peaks indicate larger lags, there are CCFs which are marginally weaker (within the error-bars) than the ones corresponding to larger lags, indicating also shorter lags; b) in all three-year periods there are small time lags (between 0.3-07 light days) which are in agreement with the one obtained in the third period, for the division based on the line profiles. Of course, we cannot exclude that some effects, for instance a contribution to the line or continuum fluxes from two different regions can cause such time lags, but the results of CCF analysis indicate at least a compact component of the BLR (0 - 2 light days) is always present.

4. Discussion

During the monitoring period, the spectrum of NGC 4151 has shown strong changes, not only in the line and continuum fluxes, but also in the Hβ and Hα line profiles. Using the line profiles, we characterized three periods (see §3.3, Tables 12 and 13, and Fig. 12). **We found that the FWHM of Hα and Hβ are different, Hβ being significantly broader than Hα (~1000 km/s). This may indicate that Hβ is formed deeper in the BLR, i.e.**
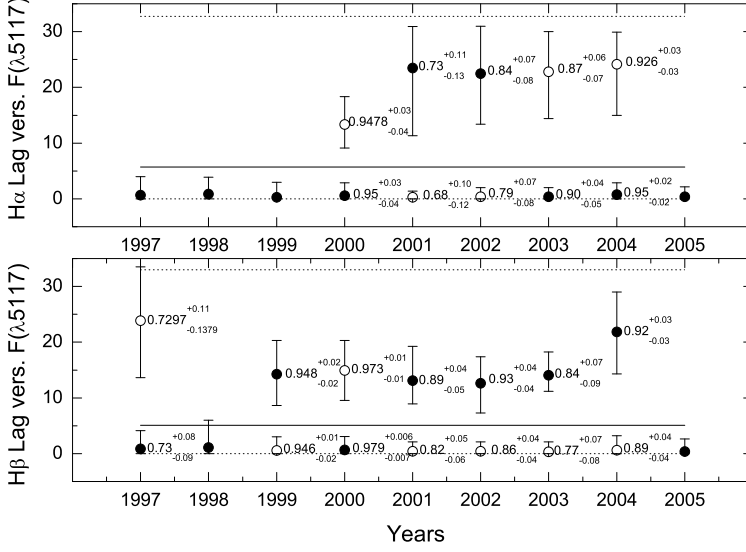
Fig. 13. The time lags obtained by binning the whole period into time intervals of three years, starting from 1996 with one year step. Full circles correspond to the maximal CCF values, and open circles to CCF values which are consistent within the error bars with the maximal one (where there are present). The time lag obtained in during the whole monitoring period is shown as a solid horizontal line, and the error-bars are shown as dashed horizontal lines.

Table 13. Time lags and CCF coefficients for the whole monitoring period, **for the three periods based on the profile shapes, and for the division based on the three values of the continuum intensity ($F_{con}^1 \geq 7 \cdot 10^{-14}$ erg cm^{-2}s^{-1}Å^{-1}; $F_{con}^1 > F_{con}^2 \geq 4 \cdot 10^{-14}$ erg cm^{-2}s^{-1}Å^{-1} and $F_{con}^3 < F_{con}^2 \geq$).** The CCF coefficients are calculated between the continuum flux and the Hα, Hβ fluxes **(line lagging contninuum). Positive time lags mean that the line light curve lags behind the continuum light curve.** The time lags are given in days.

Period	Hα	CCF	Hα-cent	Hβ	CCF	Hβ-cent
1996-2006	$5.70^{+27.05}_{-5.70}$	$0.87^{+0.02}_{-0.02}$	80.36 ± 12.93	$5.09^{+27.89}_{-5.09}$	$0.93^{+0.01}_{-0.01}$	69.79 ± 11.91
First	$0.68^{+3.30}_{-0.68}$	$0.67^{+0.09}_{-0.10}$	0.62 ± 1.11	$1.11^{+4.90}_{-1.11}$	$0.82^{+0.04}_{-0.05}$	11.61 ± 2.87
Second	$21.86^{+9.03}_{-10.53}$	$0.78^{+0.11}_{-0.14}$	66.07 ± 9.95	$11.15^{+5.00}_{-4.17}$	$0.88^{+0.06}_{-0.07}$	8.15 ± 2.38
Third	$0.81^{+1.55}_{-0.81}$	$0.94^{+0.02}_{-0.02}$	3.18 ± 1.76	$0.81^{+2.19}_{-0.81}$	$0.86^{+0.03}_{-0.04}$	16.17 ± 3.14
Continuum	Hα	CCF	Hα-cent	Hβ	CCF	Hβ-cent
F_{con}^1	$0.27^{+0.73}_{-0.27}$	$0.51^{+0.22}_{-0.27}$	–	$25.15^{+13.77}_{-20.16}$	$0.50^{+0.23}_{-0.28}$	–
F_{con}^2	$19.36^{+10.42}_{-5.44}$	$0.66^{+0.14}_{-0.17}$	0.56 ± 6.245	$0.62^{+3.49}_{-0.62}$	$0.70^{+0.07}_{-0.08}$	2.71 ± 5.22
F_{con}^3	$1.19^{+6.01}_{-1.19}$	$0.67^{+0.07}_{-0.08}$	13.65 ± 4.47	$0.70^{+2.94}_{-0.70}$	$0.82^{+0.04}_{-0.04}$	12.28 ± 5.26

closer to the Black Hole. But on the other hand, the blue asymmetry in the averaged rms of Hβ and Hα could indicate a contribution of the emitting gas with an approaching motion, i.e. an outflow. Finally, the presence of the central spike in the rms spectrum is hard to explain unless it is produced by a remote component with an axisymmetric distribution and no outward motion. A suggestion is that it comes from a region heated and ionised by the jet. In conclusion, there seems to be two BLR components, the first being closer and in outward motion, the second being located further away with no outward motions. Only the first component is permanent. Such a structure is also suggested by the time lags and the CCFs. We leave for the following paper a detailed discussion based on the study of the line profiles, and we focus here on the global line variations.

We found that the responses of the Hβ and Hα fluxes to the continuum flux were different in the three periods, but it can be due to the limited range of fluxes in periods 2 and 3. For low values of the continuum flux ($Fc \leq 6\ 10^{-14}$ erg cm^{-2}s^{-1}Å^{-1}), there was a linear relation between the lines and the continuum in the second and third periods (see Fig. 12). The dispersion of the points is larger in the second than in the third period, so we think that the results concerning the last period are more reliable. Note that Fc is smaller than $4\ 10^{-14}$ erg cm^{-2}s^{-1}Å^{-1} in period 2 and smaller than $6\ 10^{-14}$ erg cm^{-2}s^{-1}Å^{-1} in period 3, and that the linear relation seems to flatten for Hβ between 4 and $6\ 10^{-14}$ erg cm^{-2}s^{-1} in period 3. In the first period, there are only a few points for $Fc \leq 4\ 10^{-14}$ erg cm^{-2}s^{-1} and they all correspond almost to the same value of Fc, but if one interpolates between these points and those at $Fc \sim 6\ 10^{-14}$ erg cm^{-2}s^{-1}, about the same relation as in periods 2 and 3 is obtained. Still in the first period, when the continuum flux was more intense, i.e. $Fc \geq 7\ 10^{-14}$ erg cm^{-2}s^{-1}Å^{-1}, the linear relation between the line and continuum fluxes disappeared, and the line fluxes saturated at values $\sim 30\ 10^{-12}$erg cm^{-2}s^{-1} for Hα and $\sim 8\ 10^{-12}$erg cm^{-2}s^{-1} for Hβ (see Fig. 12). Note finally that if one extrapolates linearly the continuum flux to zero, e.g. in the third period, it seems that the line flux is still larger than zero, being on the order of $5 \cdot 10^{-12}$ erg cm^{-2} s^{-1} for Hα. It appears thus that the relation between the line and the continuum is not linear in the whole continuum flux range (2 to $12\ 10^{-14}$erg cm^{-2}s^{-1}), but it steepens at low fluxes and saturates at high fluxes. This could occur when the ionizing incident flux is intense, so the medium reprocesses the irradiating flux into continua (Balmer, Pashen...) and not into lines (cf. for instance Collin-Souffrin & Lasota 1988).

Let us try to model roughly the response of the lines to a given continuum flux. For the highest value of the continuum flux, one gets an optical luminosity $L_{\rm opt} = \lambda L_\lambda \sim 10^{43}$ erg s^{-1}. One can then compute the ionizing flux incident on the BLR, assuming it to be on the order of the optical flux, $F_{\rm ion} \sim L_{\rm opt}/(4\pi R^2)$, where R is the radius of the BLR (of course it is a very rough approximation; it will be refined in the following paper). Assuming an average energy of the ionizing photons $< h\nu_{\rm ion} >$ equal to 2 Rydbergs, and using the grids of models computed with Cloudy published by Korista et al. (1997) for a typical AGN spectrum (AGN3 in their list), one finds the results shown in Fig. 14. On the left panel, the Hβ fluxes at Earth are given as a function of the density, for a covering factor equal to unity, and $R = 1$ and 3 light days. On the right panel, the computed Hβ flux at the source is given as a function of the ionizing photon flux $\phi = L_{\rm ion}/(4\pi R^2 < h\nu_{\rm ion} >)$, whose minimum and maximum **recorded** values are marked as the two vertical lines. For this computation, the size of the BLR is 3 light days, and $L_{\rm ion} = 10^{43}$ ergs cm^{-3}. **From the left panel of Fig. 14**, it is clear that the observed line flux is always much larger than the computed one, even for the highest density 10^{14} cm^{-3}. **(We recall that the observed fluxes of the broad component of Hβ and Hα are: $F_{H\alpha}$=(5.1 – 31.1) 10^{-12}erg cm^{-2}s^{-1} and $F_{H\beta}$=(2.3 – 9.8) 10^{-12}erg cm^{-2}s^{-1}.) From the right panel of Fig. 14, we see that** no saturation effect appears in the computed fluxes, except for the low density 10^{10} cm^{-2}, for which the line flux is much too small (see the left panel).

There are two possibilities to account for this behavior:
(i) The ionizing flux is considerably underestimated by our assumption of equality with the optical flux. This could be linked with the fact that, in general, UV variations in Seyfert nuclei are stronger than optical ones, corresponding to a "flattening" of the spectrum when the object brightens. If the ionizing flux is under-
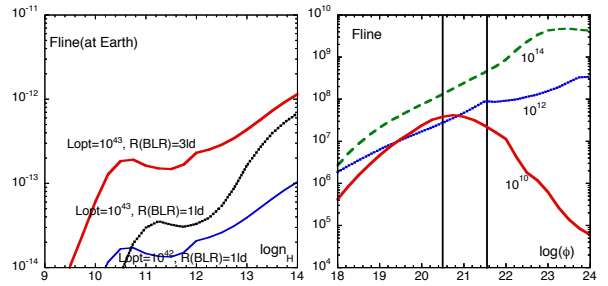
Fig. 14. Computed Hβ flux for the conditions of NGC 4151: left, at Earth, and as a function of the density in cm^{-3}; right, at the source, and as a function of the photon flux ϕ in cm^{-2} s^{-1}. The two vertical lines mark the lowest and highest values of the photon flux as defined in the text, deduced from the observations. On the right panel, the curves are labeled by the density in cm^{-3}. See the text for more explanations.

estimated, a saturation effect could appear if the BLR consists in a mixture of gas with different densities ranging from 10^{10} to 10^{14} cm^{-3} (cf. Fig. 14, right).
(ii) A non-photoionized region is contributing to the Balmer lines. Such a "mechanically heated" region was invoked by Dumont et al. (1998) to account for the strong intensities of the Balmer lines in NGC 5548. This region could be associated with the radio-jet. Indeed the radio image of NGC 4151 reveals a 0.2-pc two-sided base to the well-known arc-second radio jet (Ulvestad et al. 2005)[2]. Thus the BLR would be made of two-components: the usual one, ionized by the radiation of the accretion disc and its corona, and another component, possibly associated with a rotating outflow surrounding the jet (Murray & Chiang 1997). In this second component, ionization and heating could be due either to relativistic particles or to a shock at the basis of the jet, and they could not be directly correlated to the ionizing continuum. **This interpretation would be in agreement with the results of the study of the time lags and CCF, as well as with the behavior of the line profiles.**

It is worthwhile recalling here the results obtained from spectro-polarimetry of Hα by Martel (1998). He presented evidence that the scattering axes of different parts of the Hα profile correlate with the major morphological axes of the host galaxy of NGC 4151. If scattering is the dominant polarization mechanism in the BLR, then there are multiple lines of sight towards large-scale structures in the host galaxy, specifically the central bar, the radio jet, and the dynamical axis. Martel (1998) suggested that the line-emitting and scattering regions are cospatial, possibly in bulk flows moving along preferential axes defined by large-scale structures, such as streaming along the bar and inflow/outflow along the radio jet. In this case, the observed variability of the Hα profile and flux could be caused, at least partly, by dynamical effects, and not by a time-variable continuum source, as it is usually assumed in reverberation mapping studies.

The time lags between the continuum and the lines were $\sim$ 5 days for Hβ and Hα during the whole monitoring period, but they differ strongly in the different periods (see Fig. 13). They were small in the first and third period (0 to 2 days), and very large in the second period (10 to 20 days). The time lags of Hα and Hβ seem different in the first and second periods, but they

---

[2] Note that Arshakian et al. (2006) found a correlation between the optical continuum and the radio-jet emission variability in the case of 3C 390.3

are compatible within the precision of the results (cf. table 12). The time lags for the first period seem to be the most realistic, since the relation between the line and continuum flux is linear and well-defined, in particular for Hα. **Moreover, there were always short time lags for the three year periods (Fig. 13) indicating the presence of a permanent small component of the BLR. During some periods, we suspect the presence of a second, much larger component.** Having in mind the two possibilities mentioned above (**larger and shorter time lags**), it is possible that an additional emission in the lines (and perhaps partly in the continuum), or a weak correlation between the optical and ionizing flux, give misleading time lags in the first and in the second period (**as well as in the whole monitoring period**). All this is difficult to understand unless the BLR is complex with a structure changing with time. If it would stay unchanged, one would expect the time lags to be small when the continuum is the lowest, i.e. during the second period. On the other hand, one should keep in mind that the Hβ and Hα line profiles were different and respond differently to the continuum in the three periods. This is another proof that the BLR structure changed. So, measuring the time delays separately in the different periods is more realistic than during the whole monitoring period.

The structure of the BLR will be discussed in the following paper, in relation with the line profiles and with their variations.

5. Conclusion

We have presented the results of a 11-year (1996 - 2006) spectral monitoring of the NGC 4151 nucleus. We have investigated the continuum and line variations during this period. We have reached the following conclusions:

(a) the nucleus of NGC 4151 showed big variations of the line and continuum fluxes during the monitoring period (1996-2006). The maximum of activity took place in 1996, and there were two minima between December 2000 and May 2001 and between February 2005 and June 2005. The continuum flux changed by a factor ∼ 6, the broad Hα and Hβ changed respectively by factors ∼3.6 and ∼5. The Hα, Hγ and Heλ4686 fluxes were well correlated with the Hβ flux (Fig. 9).

(b) There was a good linear relationship between the emission line and continuum flux variations when the continuum flux Fc was $\lesssim 7 \cdot 10^{-14}$ erg cm^{-2}s^{-1}Å^{-1}. When Fc was large ($Fc \gtrsim 7 \cdot 10^{-14}$ erg cm^{-2}s^{-1}Å^{-1}) the line fluxes either were weakly correlated, or simply did not correlate at all with the continuum flux (Figs. 10 and 12).

(c) In the minimum state, the line wings were very weak and were observed only in Hβ and Hα. Thus the spectral type of the object in the monitoring period (1996-2000) changed from Sy1.8 during the minimum of activity, to Sy1.5 during the maximum (Fig. 1).

(d) The flux ratios of the blue/red wings and blue (or red) wings/core varied differently for Hα and Hβ (Fig. 4). We found three characteristic periods (1996-1999, 2000-2001 and 2002-2006) in the profile variability. The behaviour of the rms profiles in the three periods indicates that the BLR has a complex structure.

(e) From the CCF analysis, we found a time lag of about 5 days for the whole monitoring period, but it was smaller (0-2 days) in the first and the third periods, and larger (10-20 days) in the second period, implying that the dimension of the BLR varied with time. **An analysis of the time lags and CCFs for a period of three years starting from 1996 shows that short time lags are present in all periods. Therefore,** we propose

that the time lags during the third period is more realistic, since line fluxes were srtongly correlated with the continuum flux as expected if the optical is proportional to the ionizing continuum. **In summary we suspect that the BLR contains a permanent small component, and sometimes an additional component of much larger dimensions.**

(f) The lines and the continuum variations behave differently during the three periods. In the first period, when the continuum was strong, the line fluxes saturate, meaning that the optical continuum was not proportional to the ionizing continuum (Fig. 12). More generally, we found an excess of line emission with respect to a pure photoionization model during the whole monitoring period. This result could imply, either the presence of a non-radiatively heated region, or an ionizing to optical flux ratio larger than expected for a typical AGN spectrum.

A discussion of the line profiles and of the structure of the BLR will be given in a fortcoming paper (paper II).

Acknowledgments

References

Alexander, T. 1997, Astronomical Time Series, Eds. D. Maoz, A. Sternberg, and E. M. Leibowitz, (Dordrecht: Kluwer), 163.
Antonucci R.R.J. and Cohen R.D. 1983 ApJ., 271, 564
Arshakian, T G. et al. 2006, astro-ph/0602016
Bentz, M. C. et al. 2006, ApJ, 651, 775
Bochkarev N.G., Zhekov, S.A., Shapovalova, A.I. 1988, Adv.Space Res. 8, 625
Bochkarev N.G., Shapovalova A.I., Zhekov S.A., 1991, AJ, 102, 1278
Clavel, J. et al., 1990, MNRAS, 246, 668
Collin-Souffrin, S. Lasota, J.-P. 1988, PASP, 100, 1041
Dumont, A,M., Collin-Souffrin, S., and Nazarova, L. 1998, A&A, 331, 11
Edelson, R.A., Krolik, J.H. 1988, ApJ, 333, 646
Evans, I.N. et al. 1993, ApJ, 417, 82
Gaskell, C.M. & Sparke, L.S. 1986, ApJ, 305, 175
Gaskell, C.M. & Peterson, B.M. 1987, ApJS, 65, 1
Kaspi, S, Maoz, D., Netzer, H. et al. 1996, ApJ, 470, 336
Lyuty, V.M. 2005 Pis'ma in Astronom. Zhurnal 31, 723 (rus)
Malkov, Yu. F., Pronik, V.I., and Sergeev, S.G. 1997, A&A, 324, 904
Maoz, D., Netzer, H., Mazeh, T., Beck, S., Almoznino, E., Leibowitz, E., Brosch, N., Mendelson, H. and Laor, A. 1991 ApJ, 367, 493
Martel, A.R. 1998, ApJ, 508, 657.
Metzroth, K. G., Onken, C. A., & Peterson, B. M. 2006, ApJ, 647, 901
Murray, N. and Chiang, G. 1997, ApJ, 474, 91
Nazarova, L. S., Gondhalekar, P. M., Bochkarev, N. G., & Shapovalova, A. I. 1998, A&A, 331, 471
Oknyanskij, V.L.,Lyuty, V.M., Taranova, O.G., Shenavrin, V.I. 1999 Astronomy Letters, 25, 483
Penston, M.V., Perez, E., 1984, MNRAS, 211, 581
Peterson, B., M. 1988, PASP, 100, 18
Peterson, B., M. 1993, PASP, 105, 207
Peterson, B.M. et al. 1995,PASP, 107, 579
Peterson, B.M. and Cota, S.A. 1988,ApJ, 330, 111
Sergeev, S. G., Pronik, V. I., Sergeeva, E.A. 2001, ApJ, 554, 245
Shapovalova, A.I., Burenkov, A.N., Bochkarev, N.G. 1996 Bull. Spec. Astrophys. Obs., 41, 28
Shapovalova, A.I. et al. 2004, A&A, 422, 925
Ulrich, M.-H. et al. 1984 MNRAS206, 221

Ulrich, M.-H.& Horne, K., 1996 MNRAS283, 748
Ulrich, M.-H. 2000 Astro.Astrophys.Rev., 10, 135
Ulvestad, J.S., Wong, D.S., Taylor, G.B., Gallimore, J.F., Mundell, C.G. 2005,
    AJ, 130, 936.
Yaqoob T. et al. 1993 mnras, 262, 435
Van Groningen, E. & Wanders, I. 1992, PASP, 104, 700
Vlasyuk, V.V. 1993, Bull. Special Astrophys. Obs., 36, 107

Online Material

Table 3. Corrections for the position angle effect. Columns: 1 - position angle (PA) in degrees; 2 - projected spectrograph entrance apertures in arcsec; 3 - slit position angle (PA) corrections for emission lines (kp); 4 - estimated PA correction error for emission line, e(kp); 5 - position angle (PA) corrections for continuum flux, kp(cnt); 6 - the estimated PA correction error for continuum flux, e(kp(cnt));

PA deg.	Apertura arcsec	kp(Hβ)	±e	kp(cnt)	±e
1	2	3	4	5	6
90	2.0×6.0	1		1	
90	4.0×20.4	1		1	
0	2.0×6.0	0.969	0.035	0.968	0.017
0	4.0×20.4	1.011	0.018	1.019	0.009
45	2.0×6.0	1.062	0.006	1.098	0.024
45	4×20.4	1.048	0.003	1.071	0.006
135	2.0×6.0	0.954	0.018	0.943	0.011
135	4.0×20.4	0.974	0.004	0.981	0.005

Table 4. Correction for seeing effects for apertures (2"×6") and (2.5"×6"). Columns: 1 - Interval seeings in arcsec; 2 - mean seeing (arcsec); 3- our seeing correction for the emission lines fluxes, ks(our); 4 - estimated seeing correction error, e(ks); 5- Peterson's seeing correction for the emission lines fluxes from Peterson et al (1995), ks(Pet); 6 - our host galaxy seeing correction for the continuum fluxes, in units of 10^{-14} erg s^{-1} cm^{-2} Å^{-1}, Gs(our); 7 - estimated host galaxy seeing correction error, e(Gs); 8- Peterson's host galaxy seeing correction Gs(Pet) for the continuum fluxes from Peterson et al (1995);

interval seeings arcsec	Mean seeing arcsec	ks(our) (2"×6") Hβ wings	±e	ks(Pet) (2"×10") Hβ	Gs(our) (2"×6") 10^{-14}	±e	Gs(Pet) (2"×10") 10^{-14}
1	2	3	4	5	6	7	8
1"-1.5"	1.25"	0.965	0.046		-0.160	0.197	-0.070 (1.3")
	1.5"	0.977*		0.973			
1.5"-2.5"	2.0"	1.000		1.000	0		0
2.5"-3.5"	3.0"	1.042	0.030	1.052	-0.039		0.130
3.5"-4.5"	4.0"	1.069	0.063	1.086			
3.5"-5.2"					0.329	0.203	
	5"	1.096		1.105			0.31

Table 5. Corrections for the seeing effects for aperture (4.2"×19.8") Columns: 1 - Interval seeings in arcsec; 2 - mean seeing (arcsec); 3 - our seeing correction for the emission lines fluxes, ks(our); 4 - the estimated seeing correction error, e(ks); 5 - Peterson's seeing correction ks(Pet) for the emission lines fluxes from Peterson et al (1995), ks(Pet); 6 - our host galaxy seeing correction for the continuum fluxes, in units of 10^{-14} erg s^{-1} cm^{-2} Å^{-1}), Gs(our); 7 - the estimated host galaxy seeing correction error, e(Gs); 8- Peterson's host galaxy seeing correction Gs(Pet) for the continuum fluxes from Peterson et al (1995);

interval seeings arcsec	Mean seeing arcsec	ks(our) Hβ (4.2"×19.8")	±e	ks(Pet) Hβ (5"×7.5")	Gs(our) 10^{-14} (4.2"×19.8")	±e	Gs(Pet) 10^{-14} (2"×10")
1	2	3	4	5	6	7	8
2"-4"	3"	1.000		1.000	0.000		0.000
4"-6"	5"	1.063	±0.022	1.004	0.031	±0.232	0.123
4"-8"	6"	1.080	±0.035	1.015	0.188	±0.292	
6"-8"	7"	1.116					
					0.503		0.245

Table 8. The mean error (uncertainty) of our flux determinations for continuum, Hα, Hβ, Hγ and HeII 4686 emission lines in different years, and in the whole (11 years) observation period. Columns: 1 - year; 2 - ε_c, the estimated mean continuum flux error in %; 3 - sigma of the estimated mean continuum flux error in %; 4 - $\varepsilon_{H\alpha}$, the estimated mean Hα flux error in %; 5 - sigma of the estimated mean Hα flux error in %; 6 - $\varepsilon_{H\beta}$, the estimated mean Hβ flux error in %; 7 - sigma of the estimated mean Hβ flux error in %; 8 - $\varepsilon_{H\gamma}$, the estimated mean Hγ flux error in %; 9 - sigma of the estimated mean Hγ flux error in %; 10 - ε_{HeII}, the estimated mean flux error in %; 11 - sigma of the estimated mean HeII 4686 flux error in %; Bottom - mean error (uncertainty) in the whole (11 years) observation period.

Year	ε_c	$\pm\sigma$	$\varepsilon_{H\alpha}$	$\pm\sigma$	$\varepsilon_{H\beta}$	$\pm\sigma$	$\varepsilon_{H\gamma}$	$\pm\sigma$	ε_{HeII}	$\pm\sigma$
1	2	3	4	5	6	7	8	9	10	11
1996	3.9	2.27	1.9	1.2	3.90	1.56	7.5		10.4	4.20
1997	5.17	2.98	2.19	1.63	1.63	1.81	6.0	1.62	10.22	4.20
1998	2.18	1.37	3.1	2.4	1.90	1.42	5.75	1.62	10.18	4.70
1999	3.24	2.22	1.75	1.28	2.29	1.68	5.65	4.95	6.26	3.00
2000	2.3	3.65	3.62	2.31	2.12	0.82	2.88	2.53	4.65	4.47
2001	3.77	3.16	2.9	1.13	1.63	2.25	4.2	1.7	12.90	4.67
2002	2.05	1.38	2.7	1.66	3.91	2.44	5.37	5.9	5.60	1.56
2003	3.34	2.37	2.8	1.49	2.86	2.44	4.82	2.67	7.62	4.76
2004	2.65	2.26	2.6	0.8	2.25	3.18	3.85	4.45	7.28	4.57
2005	2.37	2.14	2.72	2.63	1.96	2.22	3.3	1.31	7.37	5.86
2006	2.42	1.76	2.12	1.68	1.62	1.34	6.58	1.97	8.62	4.71
mean (1996-2006)	2.84	1.23	2.46	0.75	2.37	0.84	4.99	1.46	7.78	2.51

Table 2. Log of the spectroscopic observations: Columns: 1 - UT date; 2 - Julian date (JD); 3- code according to Table 1; 4 - projected spectrograph entrance apertures; 5 - wavelength range covered; 6 - spectral resolution; 7 - slit position angle (PA) in degrees; 8 - mean seeing in arcsec.

UT-date	JD (2400000+)	Code	Apertura (arcsec)	Sp.range (Å-Å)	Res. (Å)	PA (deg)	Seeing (")
1	2	3	4	5	6	7	8
Jan. 11, 1996	+50094.5	L1(G)	4.0×12.4	3840-5600	8	33	3
Jan. 15, 1996	+50097.6	L1(G)	4.0×13.8	3640-7140	10	77	3
Jan. 16, 1996	+50098.6	L1(G)	4.0×15	3640-7140	10	90	4.5
Feb. 14, 1996	+50128.0	L(N)	1.5×6.0	3400-5440	10	211	2.4
Mar. 19, 1996	+50162.4	L(N)	2.0×6.0	3650-5540	9	235	4.8
Mar. 20, 1996	+50163.3	L(N)	2.0×6.0	4750-7340	13		3.5
Mar. 21, 1996	+50164.4	L(N)	2.0×6.0	3650-5540	8	40	1.6
Mar. 22, 1996	+50165.4	L1(G)	4.0×19.8	5700-7500	8		4
Mar. 23, 1996	+50166.3	L(N)	2.0×6.0	4750-7340	13		
Apr. 26, 1996	+50200.3	L(U)	2.0×6.0	4440-5200	5	353	2.4
Apr. 27, 1996	+50201.3	L(U)	2.0×6.0	4440-5200	5	351	1.6
Jun. 14, 1996	+50249.3	L(U)	2.0×6.0	4440-5240	5	131	2.4
Jul. 10, 1996	+50275.3	L(U)	2.0×6.0	3700-5340	10	97	1.2
Jul. 11, 1996	+50276.3	L(U)	2.0×6.0	6140-6950	6	131	1.4
Jul. 12, 1996	+50277.3	L(U)	2.0×6.0	4450-5250	5	117	1.6
Jul. 15, 1996	+50280.3	L(U)	2.0×6.0	4450-5250	5	123	1.6
Jul. 16, 1996	+50281.3	L(U)	2.0×6.0	6140-6950	6		1.3
Nov. 05, 1996	+50392.6	L(U)	2.0×6.0	4450-5250	5	27	3.2
Nov. 15, 1996	+50402.6	L(U)	2.0×6.0	3700-5400	11	349	2
Mar. 02, 1997	+50510.4	L(U)	2.0×6.0	4390-5200	5	333	2.4
Mar. 03, 1997	+50511.4	L(U)	2.0×6.0	4440-5250	5	9	2.4
Apr. 05, 1997	+50543.6	L1(G)	4.2×19.8	4140-5850	8	90	4.4
Apr. 06, 1997	+50544.4	L1(G)	4.2×19.8	4140-5800	8	90	4.4
Apr. 08, 1997	+50547.3	L(U)	2.0×6.0	4640-5450	5	353	3.2
Apr. 13, 1997	+50552.3	L(U)	2.0×6.0	4440-5250	5	337	2
Dec. 27, 1997	+50809.7	L(U)	2.0×6.0	4540-5340	5	153	1.6
Dec. 28, 1997	+50810.7	L(U)	2.0×6.0	3840-7240	15	149	4
Jan. 20, 1998	+50833.6	L(N)	2.0×6.0	3840-6150	8	141	1.2
Jan. 21, 1998	+50834.6	L(N)	2.0×6.0	3840-6150	8	142	1.2
Jan. 23, 1998	+50836.7	L(N)	2.0×6.0	4240-5500	5	131	1.2
Jan. 23, 1998	+50836.7	L(N)	2.0×6.0	3840-6150	8	130	1.2
Jan. 28, 1998	+50842.4	L(U)	2.0×6.0	4540-5350	5	357	1.6
Feb. 22, 1998	+50867.4	L(N)	2.0×6.0	3840-6150	8	352	1.2
Apr. 30, 1998	+50934.5	L1(G)	8.0×19.8	4100-5750	8	147	4.4
May. 04, 1998	+50938.3	L(N)	2.0×6.0	3740-6150	8	140	2.8
May. 07, 1998	+50940.5	L(N)	2.0×6.0	3740-6150	8	90	3.6
May. 08, 1998	+50941.5	L(N)	2.0×6.0	3740-6150	8	92	2
May. 08, 1998	+50942.5	L(N)	2.0×6.0	3740-6150	8	119	1.6
May. 08, 1998	+50942.5	L(N)	2.0×6.0	4140-5400	5	115	1.6
Jun. 20, 1998	+50985.3	L1(G)	8.0×19.8	4120-5740	8	0	4.4
Jun. 26, 1998	+50991.3	L(N)	2.0×6.0	3640-6040	8		2
Jul. 14, 1998	+51008.7	GH	2.5×6.0	3970-7210	15	90	2
Jul. 16, 1998	+51010.7	GH	2.5×6.0	3630-6890	15	90	2
Jul. 17, 1998	+51011.6	GH	2.5×6.0	4210-7470	16	90	2
Jul. 21, 1998	+51015.7	GH	2.5×6.0	4040-7280	12	90	2.7
Jul. 30, 1998	+51025.3	L(U)	2.0×6.0	4540-5350	5	120	3.6
Nov. 13, 1998	+51130.6	L1(G)	8.0×19.8	4140-5810	8	90	4.4
Dec. 19, 1998	+51166.6	L1(G)	4.0×19.8	4140-5760	8	90	6.6
Jan. 12, 1999	+51190.7	L(U)	2.0×6.0	6250-7100	9		2.5
Jan. 13, 1999	+51191.9	GH	2.5×6.0	4140-7420	15	90	1.5
Jan. 14, 1999	+51193.0	GH	2.5×6.0	4150-7430	15	90	1.3
Jan. 22, 1999	+51200.5	L1(G)	4.2×19.8	4100-5740	8	90	2.2
Jan. 23, 1999	+51201.6	L1(G)	4.2×19.8	4100-5740	8	0	4.4
Jan. 25, 1999	+51203.6	L1(G)	4.2×19.8	4100-5750	9	0	6.6
Feb. 09, 1999	+51218.6	L(U)	2.0×6.0	3640-8040	14	156	4
Feb. 12, 1999	+51221.7	L(U)	2.0×6.0	3640-7940	14	156	1.6
Feb. 13, 1999	+51222.6	L(U)	2.0×6.0	4290-5500	5	181	5.2
Feb. 14, 1999	+51223.6	L(U)	3.0×6.0	4290-5500	5	143	2.4

Table 2. Continued.

UT-date	JD (2400000+)	Code	Apertura (arcsec)	Sp.range (Å-Å)	Res. (Å)	PA (deg)	Seeing ('')
1	2	3	4	5	6	7	8
Mar. 15, 1999	+51252.9	GH	2.5×6.0	4200-7490	17	90	2.0
Mar. 20, 1999	+51258.5	L1(G)	4.2×19.8	4090-5740	8	0	2.2
Mar. 23, 1999	+51261.5	L1(G)	4.2×19.8	4090-5740	8	0	8.8
Mar. 24, 1999	+51262.3	L1(G)	4.2×19.8	5590-7300	9		4
Mar. 24, 1999	+51262.5	L(U)	2.0×6.0	4290-5450	5	62	4
Apr. 09, 1999	+51277.6	L1(G)	4.2×19.8	4090-5750	8	0	4.4
Apr. 11, 1999	+51279.5	L1(G)	4.2×19.8	4040-5740	8	0	6.6
Apr. 15, 1999	+51283.5	L1(G)	3.0×19.8	4090-5770	8	50	4.4
Jun. 14, 1999	+51344.3	L1(G)	4.2×19.8	4090-5790	8	90	4.4
Jun. 16, 1999	+51346.4	L1(G)	4.2×19.8	4090-5790	8	90	4.4
Dec. 02, 1999	+51514.6	L1(G)	4.2×19.8	4090-5700	8	90	4.4
Dec. 03, 1999	+51515.6	L1(G)	4.2×19.8	4140-5750	8	90	4.4
Dec. 05, 1999	+51517.6	L1(G)	4.2×19.8	4090-5750	8	90	4.4
Jan. 09, 2000	+51552.6	L1(G)	4.2×19.8	4090-5790	8	90	2.2
Jan. 10, 2000	+51553.6	L1(G)	4.2×19.8	5640-7310	8	90	3.0
Jan. 27, 2000	+51570.9	GH	2.5×6.0	4070-7340	13	90	3.0
Jan. 28, 2000	+51571.9	GH	2.1×6.0	4070-7340	12	90	2.5
Feb. 11, 2000	+51585.5	L1(G)	4.2×19.8	4040-5740	8	90	4.4
Feb. 14, 2000	+51588.5	L1(G)	4.2×19.8	4040-5740	8	90	6.6
Feb. 14, 2000	+51589.5	L1(G)	4.2×19.8	5590-7300	8	90	4
Feb. 26, 2000	+51600.8	GH	2.1×6.0	4560-7590	12	90	2
Feb. 27, 2000	+51601.8	GH	2.1×6.0	4300-7580	12	90	3
Apr. 03, 2000	+51638.5	L1(G)	4.2×19.8	4090-5790	8	90	4.4
Apr. 05, 2000	+51640.5	L1(G)	4.2×19.8	4040-5740	8	90	6.6
Apr. 25, 2000	+51659.8	GH	2.1×6.0	4210-7490	12	90	2.5
Apr. 26, 2000	+51660.8	GH	2.1×6.0	4210-7490	15	90	2.5
May. 11, 2000	+51676.4	L1(G)	4.2×19.8	4090-5790	10	90	4.4
May. 25, 2000	+51689.7	GH	2.5×6.0	4140-7390	15	90	2.5
May. 26, 2000	+51690.7	GH	2.5×6.0	4140-7390	15	90	3.5
Jul. 10, 2000	+51736.4	L1(G)	4.2×19.8	4060-5750	8	90	6.6
Jul. 29, 2000	+51755.3	L1(G)	4.2×19.8	4060-5750	8	90	4.4
Nov. 21, 2000	+51869.6	L(U)	2.0×6.0	4242-5398	5	90	1.2
Nov. 30, 2000	+51878.6	L1(G)	4.2×19.8	4090-5740	8	90	4.4
Dec. 17, 2000	+51895.9	GH	2.5×6.0	4010-7310	13	90	2
Dec. 18, 2000	+51897.0	GH	2.5×6.0	4010-7340	13	90	2
Dec. 19, 2000	+51898.0	GH	2.5×6.0	4000-7270	15	90	4
Jan. 26, 2001	+51936.5	L1(G)	4.2×19.8	5640-7300	8	90	2
Jan. 28, 2001	+51937.5	L1(G)	4.2×19.8	4090-5750	8	90	4.4
Jan. 31, 2001	+51940.6	L1(G)	4.2×19.8	4040-5700	8	90	4.4
Feb. 02, 2001	+51943.5	L1(G)	4.2×19.8	4140-5750	8	90	6.6
Feb. 11, 2001	+51952.4	L1(G)	4.2×19.8	4090-5750	8	0	4.4
Mar. 13, 2001	+51981.7	GH	2.5×6.0	4130-7430	14	90	2
Apr. 13, 2001	+52013.3	L1(G)	4.2×19.8	4090-5750	8	90	3.0
Apr. 16, 2001	+52016.4	L1(G)	4.2×19.8	4090-5750	8	90	4.4
Apr. 29, 2001	+52029.5	L1(G)	4.2×19.8	4090-5800	8	90	6.6
May. 05, 2001	+52034.6	GH	2.5×6.0	3600-6800	12	90	3.5
May. 06, 2001	+52036.4	L1(G)	4.2×19.8	4040-5750	8	90	4.4
May. 12, 2001	+52041.8	GH	2.5×6.0	3600-6880	15	90	1.5
May. 14, 2001	+52043.7	GH	2.5×6.0	4030-7340	13	90	2
Jun. 14, 2001	+52074.7	GH	2.5×6.0	4020-7310	13	90	3.5
Jun. 15, 2001	+52075.7	GH	2.5×6.0	4020-7310	17	90	2.5
Nov. 24, 2001	+52237.6	L(U)	2.0×6.0	3640-6000	10	91	3.6
Nov. 24, 2001	+52238.0	GH	2.5×6.0	4230-5900	8	90	2.5
Nov. 25, 2001	+52239.0	GH	2.5×6.0	5680-7380	7.5	90	2.5
Jan. 23, 2002	+52297.6	L1(G)	4.2×19.8	4040-5750	9	90	4.4
Jan. 24, 2002	+52299.4	L1(G)	4.2×19.8	4040-5750	8	90	2.2
Feb. 21, 2002	+52327.4	L1(G)	4.2×19.8	4040-5750	8	90	6.6
Feb. 22, 2002	+52327.5	L(U)	2.0×6.0	3500-5840	9	90	3.2
Mar. 05, 2002	+52338.7	GH	2.5×6.0	3900-7190	13	90	2

Table 2. Continued.

UT-date	JD (2400000+)	Code	Apertura (arcsec)	Sp.range (Å-Å)	Res. (Å)	PA (deg)	Seeing (")
1	2	3	4	5	6	7	8
Mar. 06, 2002	+52339.7	GH	2.5×6.0	5690-7390	7.5	90	2
Mar. 07, 2001	+52340.8	GH	2.5×6.0	4260-5940	8	90	2
Mar. 17, 2002	+52350.8	GH	2.5×6.0	4260-5940	8	90	3
Apr. 03, 2002	+52367.7	GH	2.5×6.0	4280-5960	8	90	2
Apr. 04, 2002	+52368.7	GH	2.5×6.0	5740-7440	7.5	90	2
Apr. 05, 2002	+52369.7	GH	2.5×6.0	3820-7130	12	90	2
Apr. 06, 2002	+52370.7	GH	2.5×6.0	3820-7130	12	90	1.5
May. 03, 2002	+52397.7	GH	2.5×6.0	4260-5940	8	90	2
May. 04, 2002	+52398.7	GH	2.5×6.0	5680-7370	7.5	90	2
May. 05, 2002	+52399.7	GH	2.5×6.0	4200-5880	8	90	2
May. 16, 2002	+52411.4	L1(G)	4.2×19.8	4090-5790	8	90	4.4
Jun. 02, 2002	+52427.7	GH	2.5×6.0	4150-5820	8	90	2.5
Jun. 04, 2002	+52429.7	GH	2.5×6.0	3990-7290	12	90	3.5
Jun. 05, 2002	+52430.7	GH	2.5×6.0	4240-5920	7.5	90	3.0
Jun. 24, 2002	+52450.4	L(U)	2.0×6.0	3500-5880	8	90	2
Dec. 11, 2002	+52620.0	GH	2.5×6.0	4230-6070	7.5	90	1.5
Dec. 12, 2002	+52621.0	GH	2.5×6.0	5750-7430	8	90	1.8
Dec. 13, 2002	+52622.0	GH	2.5×6.0	3740-7380	14	90	1.8
Dec. 14, 2002	+52623.0	GH	2.5×6.0	4240-6080	8	90	1.8
Jan. 25, 2003	+52665.0	GH	2.5×6.0	4300-5960	7.5	90	1.5
Jan. 26, 2003	+52665.9	GH	2.5×6.0	5670-7360	7.5	90	4
Jan. 27, 2003	+52666.9	GH	2.5×6.0	3920-7240	15	90	1.5
Jan. 28, 2003	+52667.9	GH	2.5×6.0	3980-7300	12	90	2.5
Mar. 25, 2003	+52723.8	GH	2.5×6.0	4240-6070	7.5	90	3.5
Mar. 26, 2003	+52724.8	GH	2.5×6.0	3747-7385	12	90	4.5
Mar. 27, 2003	+52725.8	GH	2.5×6.0	5600-7460	7.5	90	2.5
Apr. 10, 2003	+52739.7	GH	2.5×6.0	5640-7500	8	90	4
Apr. 11, 2003	+52740.8	GH	2.5×6.0	4130-5960	13	90	5.4
Apr. 12, 2003	+52741.8	GH	2.5×6.0	3700-7340	12	90	4.0
Apr. 13, 2003	+52743.3	L1(G)	4.2×19.8	5640-7330	9	90	2
May. 08, 2003	+52768.4	L1(U)	4×20.25	3750-6047	8	90	2.0
May. 08, 2003	+52768.3	L(U)	2.0×6.0	3690-6044	9	90	1.6
May. 9 , 2003	+52769.3	L(U)	2.0×6.0	3690-6044	9	90	1.5
May. 10, 2003	+52770.3	L(U)	2.0×6.0	5740-8096	8	90	1.5
May. 23, 2003	+52782.7	GH	2.5×6.0	3540-7188	12	90	3.1
May. 24, 2003	+52783.8	GH	2.5×6.0	4240-6070	7.5	90	3.5
May. 25, 2003	+52784.7	GH	2.5×6.0	5582-7450	8	90	3.7
May. 26, 2003	+52785.7	GH	2.5×6.0	4230-6075	7.5	90	2.7
Jun. 22, 2003	+52812.8	GH	2.5×6.0	4270-6970	7.5	90	1.8
Jun. 23, 2003	+52813.7	GH	2.5×6.0	5620-7330	7.5	90	1.8
Nov. 22, 2003	+52965.6	L1(G)	4.2×19.8	4089-5798	9	90	2.0
Nov. 23, 2003	+52966.6	L1(G)	4.2×19.8	4090-5748	9	90	1.5
Nov. 24, 2003	+52967.9	L1(G)	4.2×19.8	4090-5748	9	90	1.5
Dec. 22, 2003	+52995.6	L1(U)	4.0×20.2	3750-6950	10	90	3.5
Jan. 28, 2004	+53032.9	GH	2.5×6.0	4238-5950	12	90	2
Feb. 17, 2004	+53053.0	GH	2.5×6.0	3736-7120	17	90	1.6
Mar. 17, 2004	+53081.8	GH	2.5×6.0	4205-5920	12	90	2
Mar. 18, 2004	+53082.7	GH	2.5×6.0	5664-7400	14	90	
Apr. 12, 2004	+53107.6	Z2K	4.0×9.45	3784-7170	7.5	90	4.0
Apr. 13, 2004	+53108.7	GH	2.5×6.0	4216-5930	12	90	2.5
Apr. 14, 2004	+53109.7	GH	2.5×6.0	5622-7320	14	90	
May. 20, 2004	+53145.7	GH	2.5×6.0	4193-5910	12	90	2.22
May. 21, 2004	+53146.7	GH	2.5×6.0	5664-7390	7.5	90	
Jun. 12, 2004	+53168.7	GH	2.5×6.0	4208-5920	10	90	2.73
Jun. 13, 2004	+53169.7	GH	2.5×6.0	5592-7320	8	90	
Jun. 17, 2004	+53173.7	GH	2.5×6.0	4213-5920	11	90	2.50
Dec. 15, 2004	+53355.0	GH	2.5×6.0	4185-5870	7.5	90	2.96
Dec. 16, 2004	+53356.0	GH	2.5×6.0	5739-7440	7.5	90	
Dec. 18, 2004	+53357.6	L(S)	1.0×6.0	3900-7537	12.	270	1.6

Table 2. Continued.

UT-date	JD (2400000+)	Code	Apertura (arcsec)	Sp.range (Å-Å)	Res. (Å)	PA (deg)	Seeing (")
1	2	3	4	5	6	7	8
Dec. 22, 2004	+53361.5	L(S)	1.0×6.0	3900-7537	14	270	2.5
Jan. 16, 2005	+53386.9	GH	2.5×6.0	3707-7096	12	90	3.05
Jan. 17, 2005	+53388.0	GH	2.5×6.0	4183-5900	9	90	2.4
Jan. 18, 2005	+53388.9	GH	2.5×6.0	5577-7320	12	90	
Feb. 07, 2005	+53408.8	S-P	2.5×6.0	5722-7590	6.5	90	2.3
Feb. 15, 2005	+53416.9	S-P	2.5×6.0	3708-5807	7	90	2.5
Feb. 15, 2005	+53417.5	L1(U)	4.0×9.45	3750-7400	8	90	4.0
Mar. 17, 2005	+53446.8	GH	2.5×6.0	5557-7300	13	90	
Mar. 18, 2005	+53447.8	GH	2.5×6.0	3689-7090	13	90	3.0
Mar. 21, 2005	+53451.3	L1(U)	4.0×9.45	3750-7400	9	90	8
Apr. 13, 2005	+53474.4	L1(U)	4.0×9.45	3750-7400	8	90	2.5
Apr. 15, 2005	+53475.8	GH	2.5×6.0	4245-5960	9	90	2.82
Apr. 16, 2005	+53476.8	GH	2.5×6.0	5521-7256	10	90	
Apr. 16, 2005	+53477.3	L1(U)	4.0×9.45	3750-7400	8	90	5.5
Apr. 18, 2005	+53478.7	GH	2.5×6.0	3745-7190	13	90	
May. 12, 2005	+53503.3	L1(U)	4.0×9.45	3750-7400	8	90	2.0
May. 13, 2005	+53503.7	GH	2.5×6.0	4216-5910	9	90	3.0
May. 14, 2005	+53504.7	GH	2.5×6.0	5583-7300	7	90	
May. 16, 2005	+53507.4	L1(U)	4.0×9.45	3750-7400	8	90	3.2
Jun. 09, 2005	+53530.7	GH	2.5×6.0	3714-7070	12	90	1.94
Jun. 10, 2005	+53531.6	GH	2.5×6.0	4274-5970	9	90	3.37
Jun. 11, 2005	+53531.6	GH	2.5×6.0	5676-7395	7.5	90	
Jun. 16, 2005	+53538.3	L1(U)	4.0×9.45	3740-7350	9	90	2.5
Nov. 28, 2005	+53703.0	GH	2.5×6.0	3590-6900	15	90	3.0
Nov. 29, 2005	+53704.0	GH	2.5×6.0	4230-5910	7	90	2.8
Dec. 06, 2005	+53711.0	S-P	2.5×6.0	3690-5780	7	90	2.5
Dec. 07, 2005	+53712.0	S-P	2.5×6.0	3690-5780	7	90	2.5
Dec. 27, 2005	+53732.0	GH	2.5×6.0	3890-7270	17	90	3
Dec. 28, 2005	+53733.0	GH	2.5×6.0	3880-7260	17	90	2.4
Jan. 21, 2006	+53756.9	GH	2.5×6.0	4330-6040	9	90	2.7
Jan. 22, 2006	+53757.9	GH	2.5×6.0	4330-6040	9	90	3
Jan. 24, 2006	+53760.5	L1(U)	4.0×9.45	3740-7400	9	90	3.5
Jan. 25, 2006	+53761.5	L1(U)	4.0×9.45	3740-7400	9	90	2.5
Feb. 20, 2006	+53786.9	GH	2.5×6.0	3740-7120	17	90	2.8
Feb. 21, 2006	+53787.5	L1(U)	4.0×9.45	3740-7400	8	90	2
Feb. 22, 2006	+53788.5	L1(U)	4.0×9.45	3740-7400	8	90	2
Feb. 23, 2006	+53789.5	GH	2.5×6.0	3740-7400	15	90	2.5
Mar. 09, 2006	+53803.8	GH	2.5×6.0	3730-7100	14	90	5.1
Mar. 21, 2006	+53816.4	L1(U)	4.0×9.45	3740-7400	8	90	5
Mar. 22, 2006	+53817.4	L1(U)	4.0×9.45	3740-7400	8	90	4
Apr. 18, 2006	+53843.7	GH	2.5×6.0	3720-7090	9	90	2.7
Apr. 19, 2006	+53844.8	GH	2.5×6.0	4240-5940	7	90	2.5
Apr. 20, 2006	+53845.7	GH	2.5×6.0	4240-5940	7	90	2.1
Apr. 20, 2006	+53846.4	L1(U)	4.0×9.45	3740-7400	8	90	2.5

Table 7. Observed continuum, Hα, Hβ, Hγ and HeIIλ4686 fluxes, reduced to the 6 m telescope aperture $2'' \times 6''$. The fluxes are corrected for position angle (to PA=90 degree), seeing and aperture effects. Columns: 1 - Julian date; 2 - F(cont), the continuum flux at 5117 Å (in units of 10^{-14} erg s^{-1} cm^{-2} Å^{-1}); and ε_{cont}, the estimated continuum flux error; 3 - F(Hα), the Hα total flux (in units of 10^{-12} erg s^{-1} cm^{-2}), and $\varepsilon_{H\alpha}$, the Hα flux error; 4 - F(Hβ), the Hβ total flux (in units of 10^{-12} erg s^{-1} cm^{-2}), and $\varepsilon_{H\beta}$, the Hβ flux error; 5 - F(Hγ), the Hγ total flux (in units of 10^{-12} erg s^{-1} cm^{-2}), and $\varepsilon_{H\gamma}$, the Hγ flux error; 6 - F(HeII), the HeIIλ4686 total flux (in units of 10^{-12} erg s^{-1} cm^{-2}), and ε_{HeII}, the HeIIλ4686 flux error.

JD	F(cont) $\pm \varepsilon_{cont}$	F(Hα) $\pm \varepsilon_{H\alpha}$	F(Hβ) $\pm \varepsilon_{H\beta}$	F(Hγ) $\pm \varepsilon_{H\gamma}$	F(HeII) $\pm \varepsilon_{HeII}$
50094.5	8.8 ±0.34	– –	8.03±0.31	4.807±0.361	3.136± 0.031
50097.6	9.26 ±0.36	33.41±0.63	8.19±0.32	3.893±0.292	2.707± 0.027
50098.6	9.26 ±0.36:	35.16±0.63	– –	– –	– –
50128	11.25 ±0.44	34.34±0.65	9.28±0.36	4.524±0.339	3.495± 0.035
50162.4	11.66 ±0.45	– –	8.9 ±0.35	3.638±0.273	2.22 ± 0.022
50163.3	11.66 ±0.45:	33.79±0.64	– –	– –	– –
50164.4	10.78 ±0.42	– –	8.5 ±0.33	4.044±0.303	3.485± 0.035
50165.4	10.78 ±0.42:	33.24±0.63	– –	– –	– –
50166.3	10.78 ±0.42:	32.04±0.61	– –	– –	– –
50200.3	9.6 ±0.37	– –	9.34±0.36	– –	– –
50201.3	8.85 ±0.35	30.97±0.59	8.73±0.34	– –	– –
50249.3	12.64 ±0.49	35.45±0.67	8.24±0.32	– –	– –
50275.3	11.99 ±0.47	35.72±0.68	9.83±0.38	4.649±0.349	3.313± 0.033
50276.3	11.99 ±0.47:	35.88±0.68	– –	– –	– –
50277.3	11.29 ±0.44	36.6 ±0.70	9.26±0.36	– –	– –
50280.3	12.19 ±0.48	35.95±0.68	10 ±0.39	– –	– –
50281.3	12.19 ±0.48:	35.53±0.68	– –	– –	– –
50392.6	10.04 ±0.39	– –	9.97±0.39	– –	– –
50402.6	10.65 ±0.42	39.95±0.76	10.8 ±0.42	5.003±0.375	3.792± 0.038
50510.4	7.84 ±0.41	32.4 ±0.81	9.08±0.15	– –	– –
50511.4	8.86 ±0.46	– –	9.57±0.15	– –	– –
50543.6	6.82 ±0.35	32.15±0.80	7.44±0.12	3.336±0.200	2.088± 0.021
50544.4	6.47 ±0.34	32.54±0.81	7.35±0.12	– –	– –
50547.3	6.92 ±0.36	– –	7 ±0.11	– –	– –
50552.3	7.38 ±0.38	– –	8.5 ±0.14	– –	– –
50809.7	7.56 ±0.39	– –	9.07±0.15	– –	– –
50810.7	7.22 ±0.38	– –	9.04±0.14	– –	– –
50833.6	5.91 ±0.13	31.65±0.98	7.31±0.14	3.256±0.189	1.912± 0.019
50834.6	6.09 ±0.13	31.03±0.96	7.54±0.14	3.466±0.201	2.12 ± 0.021
50836.7	6.4 ±0.14	– –	7.33±0.14	3.837±0.223	2.745± 0.027
50836.7	6.42 ±0.14	– –	7.82±0.15	3.619±0.210	2.524± 0.025
50842.4	6.59 ±0.14	32.87±1.02	8.02±0.15	– –	– –
50867.4	6.22 ±0.14	33.34±1.03	7.34±0.14	3.363±0.195	2.445± 0.024
50934.5	6.39 ±0.14	33.14±1.03	7.06±0.13	– –	– –
50938.3	6.55 ±0.14	33.6 ±1.04	6.77±0.13	2.643±0.153	1.902± 0.019
50940.5	6.27 ±0.14	30.78±0.95	6.82±0.13	2.878±0.167	1.457± 0.015
50941.5	5.64 ±0.12	– –	6.41±0.12	2.608±0.151	1.135± 0.011
50942.5	5.7 ±0.13	29.87±0.93	6.42±0.12	2.432±0.141	1.516± 0.015
50942.5	6.09 ±0.13	– –	6.25±0.12	2.653±0.154	1.157± 0.012
50985.3	8.52 ±0.19	34.03±1.05	8.29±0.16	3.118±0.181	2.738± 0.027
50991.3	7.43 ±0.16	– –	8.24±0.16	3.692±0.214	2.946± 0.029
51008.7	5.84 ±0.13	31.09±0.96	7.44±0.14	3.355±0.195	1.743± 0.017
51010.7	5.98 ±0.13	28.62±0.89	7.59±0.14	3.677±0.213	2.173± 0.022
51011.6	5.81 ±0.13	28.82±0.89	7.47±0.14	3.258±0.189	1.974± 0.020
51015.7	6.26 ±0.14	31.15±0.97	7.84±0.15	3.637±0.211	1.829± 0.018
51025.3	6.21 ±0.14	30.15±0.93	7.45±0.14	– –	– –
51130.6	5.69 ±0.13	32.59±1.01	7.05±0.13	– –	– –
51166.6	4.26 ±0.09	33.07±1.03	6.96±0.13	– –	– –
51190.7	5.56 ±0.18:	29.56±0.53	– –	– –	– –
51191.9	5.56 ±0.18	28.47±0.51	6.85±0.16	3.54 ±0.202	2.377± 0.150
51193	5.81 ±0.19	28.47±0.51	6.6 ±0.15	3.465±0.198	2.62 ± 0.165
51200.5	6.07 ±0.19	– –	7.36±0.17	– –	– –
51201.6	6.42 ±0.21	33.51±0.60	7.91±0.18	– –	– –
51203.6	6.57 ±0.21	34.83±0.63	8.05±0.19	– –	– –
51218.6	6.43 ±0.21	35.24±0.63	7.86±0.18	3.74 ±0.213	2.888± 0.182
51221.7	6.38 ±0.20	36.73±0.66	8.09±0.19	3.452±0.197	3.043± 0.192

Table 7. Continued.

JD	F(cont) $\pm\ \varepsilon_{cont}$	$F(H\alpha) \pm \varepsilon_{H\alpha}$	$F(H\beta) \pm \varepsilon_{H\beta}$	$F(H\gamma) \pm \varepsilon_{H\gamma}$	$F(HeII) \pm \varepsilon_{HeII}$
51222.6	6.06 ±0.19	– –	7.92±0.18	– –	– –
51223.6	5.69 ±0.18	– –	7.34±0.17	– –	– –
51252.9	5.03 ±0.16	29.45±0.53	6.16±0.14	2.886±0.165	1.883± 0.119
51258.5	5.79 ±0.19	32.55±0.59	6.95±0.16	– –	– –
51261.5	5.81 ±0.19	31.19±0.56	6.93±0.16	– –	– –
51262.3	5.77 ±0.18:	31.47±0.57	– –	– –	– –
51262.5	5.77 ±0.18	32.2 ±0.58	7.12±0.16	– –	– –
51277.6	5.79 ±0.19	– –	7.6 ±0.17	3.425±0.195	3.217± 0.203
51279.5	5.5 ±0.18	34.91±0.63	7.51±0.17	– –	– –
51283.5	5.29 ±0.17	– –	6.56±0.15	– –	– –
51344.3	2.87 ±0.09	– –	4.2 ±0.10	1.716±0.098	0.998± 0.063
51346.4	2.75 ±0.09	– –	4.29±0.10	2.212±0.126	1.092± 0.069
51514.6	2.77 ±0.09	– –	3.52±0.08	1.668±0.095	1.252± 0.079
51515.6	2.79 ±0.09	22.94±0.41	3.6 ±0.08	1.58 ±0.090	1.193± 0.075
51517.6	3.1 ±0.10	– –	3.47±0.08	1.574±0.090	1.391± 0.088
51552.6	4.16 ±0.10	– –	4.51±0.09	– –	– –
51553.6	4.16 ±0.10:	25.93±0.93	– –	– –	– –
51570.9	3.86 ±0.09	25.13±0.90	– –	– –	– –
51571.9	3.86 ±0.09	23.57±0.85	4.67±0.10	2.257±0.065	1.035± 0.049
51585.5	3.56 ±0.08	– –	4.16±0.09	2.615±0.076	1.52 ± 0.071
51588.5	3.6 ±0.08	– –	4.48±0.09	2.021±0.059	1.517± 0.071
51589.5	3.6 ±0.08:	24.12±0.87	– –	– –	– –
51600.8	2.78 ±0.06	22.51±0.81	4.01±0.08	– –	– –
51601.8	2.77 ±0.06	22.28±0.80	4.15±0.09	– –	– –
51638.5	2.53 ±0.06	– –	3.7 ±0.08	– –	– –
51640.5	2.3 ±0.05	– –	3.57±0.07	– –	– –
51659.8	2.63 ±0.06	20.19±0.73	3.6 ±0.08	1.88 ±0.055	1.156± 0.054
51660.8	2.61 ±0.06	19.04±0.69	3.56±0.07	1.943±0.056	1.144± 0.054
51676.4	1.88 ±0.04	– –	3.23±0.07	– –	– –
51689.7	1.95 ±0.04	17.89±0.64	3.09±0.06	1.678±0.049	0.649± 0.031
51690.7	1.92 ±0.04	19.68±0.71	3.01±0.06	1.528±0.044	0.711± 0.033
51736.4	2.31 ±0.05	– –	3.22±0.07	– –	– –
51755.3	2.72 ±0.06	– –	3.35±0.07	– –	– –
51869.6	1.86 ±0.04	– –	3.84±0.08	2.061±0.060	0.844± 0.040
51878.6	1.51 ±0.03	– –	3.14±0.07	1.687±0.049	0.918± 0.043
51895.9	1.7 ±0.04	15.92±0.57	2.49±0.05	1.203±0.035	0.71 ± 0.033
51897	1.7 ±0.04	16.61±0.60	2.55±0.05	1.18 ±0.034	0.698± 0.033
51898	1.79 ±0.04	16.22±0.58	2.64±0.06	1.2 ±0.035	0.806± 0.038
51936.5	1.79 ±0.07:	20.81±0.60	– –	– –	– –
51937.5	1.79 ±0.07	– –	2.96±0.05	– –	– –
51940.6	1.81 ±0.07	18.73±0.54	2.91±0.05	– –	– –
51943.5	1.76 ±0.07	20.09±0.58	2.94±0.05	– –	– –
51952.4	1.31 ±0.05	– –	2.75±0.04	– –	– –
51981.7	1.71 ±0.06	14.31±0.41	2.32±0.04	1.11 ±0.047	0.625± 0.008
52013.3	2.24 ±0.09	15.86±0.46	2.47±0.04	– –	– –
52016.4	2.6 ±0.10	17.27±0.50	2.63±0.04	– –	– –
52029.5	1.78 ±0.07	– –	2.79±0.04	– –	– –
52034.6	1.8 ±0.07	12.97±0.38	2.46±0.04	1.127±0.047	0.684± 0.009
52036.4	1.93 ±0.07	– –	2.61±0.04	1.217±0.051	0.86 ± 0.011
52041.8	1.83 ±0.07	13.31±0.39	2.26±0.04	1.107±0.046	0.696± 0.009
52043.7	1.99 ±0.08	13.71±0.40	2.25±0.04	1.155±0.049	0.608± 0.008
52074.7	2.68 ±0.10	17.38±0.50	3.41±0.05	1.667±0.070	0.687± 0.009
52075.7	2.84 ±0.11	15.08±0.44	3.13±0.05	1.539±0.065	0.798± 0.010
52237.6	3.34 ±0.13	21.66±0.63	5.06±0.08	2.221±0.093	1.432± 0.019
52238	3.33 ±0.13	– –	5.12±0.08	– –	– –
52239	3.33 ±0.13:	20.55±0.60	– –	– –	– –
52297.6	3.45 ±0.07	– –	4.23±0.16	– –	– –
52299.4	3.68 ±0.08	19.87±0.54	3.95±0.15	– –	– –
52327.4	3.21 ±0.07	– –	3.86±0.15	– –	– –
52327.5	3.14 ±0.07	– –	3.89±0.15	1.35 ±0.073	0.988± 0.055
52338.7	4.17 ±0.09	19.93±0.54	3.99±0.16	1.773±0.096	1.378± 0.077

Table 7. Continued.

JD	F(cont) $\pm \varepsilon_{cont}$	$F(H\alpha) \pm \varepsilon_{H\alpha}$	$F(H\beta) \pm \varepsilon_{H\beta}$	$F(H\gamma) \pm \varepsilon_{H\gamma}$	$F(HeII) \pm \varepsilon_{HeII}$
52339.7	4.17 ±0.09:	21.14±0.57	– –	– –	– –
52340.8	3.96 ±0.08	– –	4.42±0.17	– –	– –
52350.8	2.74 ±0.06	– –	4.03±0.16	1.666±0.090	0.755± 0.042
52367.7	3.94 ±0.08	– –	3.83±0.15	– –	– –
52368.7	3.94 ±0.08:	19.06±0.51	– –	– –	– –
52369.7	3.79 ±0.08	19.39±0.52	3.73±0.15	1.605±0.087	0.863± 0.048
52370.7	3.91 ±0.08	19.29±0.52	3.93±0.15	1.671±0.090	0.911± 0.051
52397.7	3.3 ±0.07	– –	3.89±0.15	1.368±0.074	0.622± 0.035
52398.7	3.3 ±0.07:	18.82±0.51	– –	– –	– –
52399.7	3.27 ±0.07	– –	3.72±0.15	1.347±0.073	0.568± 0.032
52411.4	3.84 ±0.08	– –	4.04±0.16	– –	– –
52427.7	3.72 ±0.08	– –	4 ±0.17	1.447±0.078	0.693± 0.039
52429.7	3.71 ±0.08	20.55±0.55	4.34±0.17	1.718±0.093	0.762± 0.043
52430.7	3.75 ±0.08	– –	4.04±0.16	– –	– –
52450.4	4.24 ±0.09	21.93±0.59	4.5 ±0.18	1.571±0.085	1.325± 0.074
52620	3.36 ±0.07	– –	4.29±0.17	– –	– –
52621	3.36 ±0.07:	19.15±0.52	– –	– –	– –
52622	3.44 ±0.07	19.95±0.54	4.32±0.17	1.914±0.103	0.769± 0.043
52623	3.58 ±0.08	– –	4.76±0.19	– –	– –
52665	5.07 ±0.17	– –	4.79±0.14	– –	– –
52665.9	5.07 ±0.17:	24.08±0.67	– –	– –	– –
52666.9	5.07 ±0.17	22.26±0.62	4.79±0.14	2.027±0.097	1.21 ± 0.092
52667.9	5.57 ±0.18	23.24±0.65	4.96±0.14	2.246±0.108	1.364± 0.104
52723.8	4.54 ±0.15	– –	5.35±0.16	2.304±0.111	1.227± 0.093
52724.8	4.17 ±0.14	22.59±0.63	4.96±0.14	2.277±0.109	1.369± 0.104
52725.8	4.17 ±0.14:	21.54±0.60	– –	– –	– –
52739.7	5.17 ±0.17:	23.31±0.65	– –	– –	– –
52740.8	5.17 ±0.17	– –	5.97±0.17	2.729±0.131	1.347± 0.102
52741.8	5.15 ±0.17	23.5 ±0.66	5.36±0.16	2.603±0.125	1.65 ± 0.125
52743.3	5.15 ±0.17:	22.47±0.63	– –	– –	– –
52768.4	5.16 ±0.17	– –	5.67±0.16	– –	– –
52768.3	5.08 ±0.17	– –	5.44±0.16	2.173±0.104	1.277± 0.097
52769.3	5.33 ±0.18	24.39±0.68	5.57±0.16	2.064±0.099	1.353± 0.103
52770.3	5.33 ±0.18:	23.29±0.65	– –	– –	– –
52782.7	5.03 ±0.17	24.98±0.70	5.82±0.17	2.488±0.119	1.387± 0.105
52783.8	5.17 ±0.17	– –	5.47±0.16	2.714±0.130	1.374± 0.104
52784.7	5.55 ±0.17:	23.56±0.66	– –	– –	– –
52785.7	5.55 ±0.18	– –	5.31±0.15	– –	– –
52812.8	4.18 ±0.14	– –	5.74±0.17	2.467±0.118	1.429± 0.109
52813.7	4.18 ±0.14:	22.76±0.64	– –	– –	– –
52965.6	3.68 ±0.12	– –	4.79±0.14	– –	– –
52966.6	3.46 ±0.11	– –	4.87±0.14	2.428±0.117	1.371± 0.104
52967.9	3.3 ±0.11	– –	4.83±0.14	2.709±0.130	1.588± 0.121
52995.6	3.52 ±0.12	– –	5.55±0.16	2.504±0.120	2.258± 0.172
53032.9	3.26 ±0.09	– –	4.38±0.10	2.111±0.082	0.849± 0.062
53053	3.19 ±0.09	20.35±0.53	4.92±0.11	2.405±0.094	1.4 ± 0.102
53081.8	2.76 ±0.08	– –	4.18±0.10	1.861±0.073	0.695± 0.051
53082.7	2.76 ±0.08:	17.91±0.47	– –	– –	– –
53107.6	2.03 ±0.06:	16.54±0.43	– –	– –	– –
53108.7	2.03 ±0.06	– –	3.04±0.70	1.432±0.056	0.452± 0.033
53109.7	2.03 ±0.06:	16.14±0.42	– –	– –	– –
53145.7	1.92 ±0.05	– –	2.64±0.06	1.18 ±0.046	0.585± 0.043
53146.7	1.92 ±0.05:	14.7 ±0.38	– –	– –	– –
53168.7	2.29 ±0.07	– –	2.74±0.06	1.088±0.042	0.601± 0.044
53169.7	2.29 ±0.07:	14.21±0.37	– –	– –	– –
53173.7	2.7 ±0.08	– –	2.76±0.06	1.338±0.052	0.607± 0.044
53355	2.85 ±0.08	– –	3.72±0.09	1.618±0.063	0.857± 0.061
53356	2.85 ±0.08:	18.13±0.47	– –	– –	– –
53357.6	2.85 ±0.08	18.91±0.49	3.71±0.09	1.466±0.057	0.799± 0.058
53361.5	2.81 ±0.08	17.85±0.46	3.48±0.08	1.481±0.058	0.616± 0.045
53386.9	2.56 ±0.06	19.21±0.52	3.84±0.08	1.736±0.057	0.756± 0.056

Table 7. Continued.

JD	$F(\text{cont}) \pm \varepsilon_{cont}$	$F(H\alpha) \pm \varepsilon_{H\alpha}$	$F(H\beta) \pm \varepsilon_{H\beta}$	$F(H\gamma) \pm \varepsilon_{H\gamma}$	$F(HeII) \pm \varepsilon_{HeII}$
53388	2.57 ±0.06	– –	3.79±0.08	1.692±0.056	0.625± 0.046
53388.9	2.57 ±0.06:	17.64±0.48	– –	– –	– –
53408.8	2.3 ±0.06:	16.94±0.46	– –	– –	– –
53416.9	2.04 ±0.05	– –	2.96±0.06	1.294±0.043	0.639± 0.047
53417.5	2.04 ±0.05:	16.36±0.44	– –	– –	– –
53446.8	1.92 ±0.05:	16.16±0.44	– –	– –	– –
53447.8	1.92 ±0.05	16.62±0.45	3.07±0.06	1.376±0.045	0.716± 0.053
53451.3	2.14 ±0.05	16.8 ±0.45	3.1 ±0.06	– –	– –
53474.4	1.73 ±0.05:	14.01±0.38	– –	– –	– –
53475.8	1.73 ±0.04	– –	2.47±0.05	1.014±0.033	0.62 ± 0.046
53476.8	1.73 ±0.04:	13.97±0.38	– –	– –	– –
53477.3	1.78 ±0.04:	15.77±0.43	– –	– –	– –
53478.7	1.83 ±0.04	15.08±0.41	2.42±0.05	1.071±0.035	0.684± 0.051
53503.3	2.16 ±0.05	14.79±0.40	2.51±0.05	– –	– –
53503.7	2.16 ±0.05	– –	2.74±0.05	1.241±0.041	0.796± 0.059
53504.7	2.16 ±0.05:	14.65±0.40	– –	– –	– –
53507.4	2.1 ±0.05	15.76±0.43	2.6 ±0.05	– –	– –
53530.7	1.89 ±0.05	15.07±0.41	2.62±0.05	1.168±0.039	0.681± 0.050
53531.6	1.94 ±0.05	– –	2.74±0.05	– –	– –
53531.6	1.94 ±0.05:	14.92±0.40	– –	– –	– –
53538.3	1.74 ±0.04	13.25±0.36	2.49±0.05	1.207±0.040	0.93 ± 0.069
53703	3.73 ±0.09	18.92±0.51	4.42±0.09	– –	– –
53704	3.57 ±0.09	– –	4.44±0.09	1.577±0.052	1.357± 0.100
53711	3.04 ±0.07	– –	4.3 ±0.09	2.071±0.068	1.036± 0.077
53712	2.79 ±0.07	– –	4.32±0.09	2.197±0.073	1.01 ± 0.075
53732	2.41 ±0.06	15.84±0.43	3.49±0.07	1.733±0.057	0.904± 0.067
53733	2.45 ±0.06	16.01±0.43	3.39±0.07	– –	– –
53756.9	1.88 ±0.05	– –	3.14±0.05	– –	– –
53757.9	1.92 ±0.05	– –	3.16±0.05	– –	– –
53760.5	1.8 ±0.04	15.62±0.33	2.81±0.04	– –	– –
53761.5	1.82 ±0.04	16.59±0.35	2.89±0.05	1.372±0.091	0.845± 0.073
53786.9	2.07 ±0.05	15.64±0.33	3.16±0.05	1.69 ±0.112	0.767± 0.066
53787.5	1.91 ±0.05	16.57±0.35	3.31±0.05	1.775±0.117	0.982± 0.084
53788.5	1.94 ±0.05	16.39±0.34	3.31±0.05	1.544±0.102	0.876± 0.075
53789.5	1.94 ±0.05:	16.55±0.35	– –	1.724±0.114	1.027± 0.088
53803.8	3.25 ±0.08	16.9 ±0.35	3.43±0.05	1.684±0.111	1.087± 0.093
53816.4	3.22 ±0.08	17.83±0.37	3.98±0.06	1.843±0.122	1.471± 0.127
53817.4	3.06 ±0.07	17.79±0.37	4.04±0.06	1.755±0.116	1.571± 0.135
53843.7	3.53 ±0.08	19.68±0.41	4.55±0.07	2.34 ±0.154	1.407± 0.121
53844.8	3.41 ±0.08	– –	4.52±0.07	2.071±0.137	1.458± 0.125
53845.7	3.32 ±0.08	– –	4.38±0.07	2.054±0.136	1.58 ± 0.136
53846.4	3.31 ±0.08	19.01±0.40	4.6 ±0.07	2.083±0.137	1.887± 0.162